
ELSEVIER
Volume 301, Issues 1–2
3 January 2011
ISSN 0012-821X
EARTH
& PLANETARY
SCIENCE LETTERS
Editors
Rick Carlson, Washington, DC
Peter B. deMenocal, Palisades, NY
T. Mark Harrison, Los Angeles, CA
Yanick Ricard, Lyon
P. Shearer, La Jolla, CA
Tilman Spohn, Berlin
Lars Stixrude, London

Earth and Planetary Science Letters 311 (2011) 396–410

Contents lists available at SciVerse ScienceDirect

Earth and Planetary Science Letters

journal homepage: www.elsevier.com/locate/epsl

Temperature dependence of organic matter remineralization in deeply-buried marine sediments

David J. Burdige *

Dept. of Ocean, Earth and Atmospheric Sciences, Old Dominion University, Norfolk, VA 23539, United States

ARTICLE INFO

Article history:
Received 26 January 2011
Received in revised form 20 September 2011
Accepted 26 September 2011
Available online xxxx

Editor: P. DeMenocal

Keywords:
temperature
methane
deep marine biosphere
gas hydrates
reactive transport models

ABSTRACT

Assuming that the temperature dependence of sediment organic matter remineralization can be described by the Arrhenius equation, organic matter that is highly refractory at seafloor temperatures (~2–3 °C) should become more reactive at sediment depths of several hundred meters due to burial and heating by the natural geothermal gradient. Results obtained using a coupled non-linear reactive-transport model support this suggestion. For deeply-buried marine sediments (i.e., those found 100s of meters below the seafloor) model results predict the occurrence of a deep zone of methanogenesis that is separated by a relatively thick region in which methane diffuses upwards to be oxidized by downward diffusing sulfate. This depth zonation of biogeochemical processes in deeply-buried sediments is in sharp contrast to that observed in nearshore marine sediments where sulfate reduction and methanogenesis generally occur in much closer vertical proximity. Model results presented here also provide a simple mechanistic explanation for the occurrence of linear pore water sulfate profiles that are common in many continental margin sediments. Linear sulfate gradients are often taken as an indirect indicator of gas hydrate occurrence although results presented here suggest that this does not necessarily always have to be the case. Application of the model to gas hydrate-containing sediments on the Blake Ridge yields results that are in good agreement with sediment and pore water data, and microbial rate studies in these sediments. Model results also suggest that in situ methanogenesis in and/or near the gas hydrate stability zone may play an important role in supplying the methane found in Blake Ridge gas hydrates.

1. Introduction

Deeply-buried marine sediments (i.e., found 100s of meters below the seafloor) have been isolated from the sediment surface for 10s of millions of years under pressures of 100s of atm (or ~10^4–10^5 kPa). However despite the extreme conditions in these sediments, they represent the largest prokaryotic habitat on Earth (Whitman et al., 1998). Organisms living in these sediments have extremely low rates of metabolism (e.g., D'Hondt et al., 2002), due to the fact that energy flow to these environments in terms of organic matter flux from the sediment surface is extremely low (Parkes and Sass, 2009; Schrenk et al., 2010). Furthermore, the organic matter found in these sediments is thought to be extremely refractory based on empirical observations which show that organic matter reactivity decreases with age and burial of the material (Middelburg, 1989). Past studies of deeply-buried marine sediments have examined the potential rates and the distribution of biogeochemical processes in these sediments (D'Hondt et al., 2005; Parkes et al., 1994, 2005; Wellsbury et al., 1997). Recent studies have also quantified rates of processes in these sediments using reactive-transport (advection/diffusion/reaction) models applied to sediment pore water profiles (Sivan et al., 2007; Wallmann et al., 2006; Wang et al., 2008; Wortmann, 2006).

Many deeply buried marine sediments, particularly those on the continental slope and rise, also contain methane gas hydrates, i.e., ice-like solids in which methane is trapped in a cage, or lattice, of water molecules (Bohrmann and Torres, 2006; Buffett and Archer, 2004; Davie and Buffett, 2003a; Milkov, 2004). The $\delta^{13}C$ and δD values of the methane found in gas hydrates are generally extremely light, indicating that the gas is primarily of biogenic origin (Bohrmann and Torres, 2006; Borowski et al., 1997; Hoehler et al., 2000). Previous thermodynamic and reactive transport models have successfully described many aspects of gas hydrate dynamics (Davie and Buffett, 2003a; Egeberg and Dickens, 1999; Hensen and Wallmann, 2005; Rempel and Buffett, 1997; Torres et al., 2004; Xu and Ruppel, 1999), although they do not necessarily directly relate gas hydrate dynamics to the microbial processes that produce and consume methane.

One fundamental aspect of deeply-buried sediments that has not, to my knowledge been directly incorporated into any of the reactive-transport models cited above is the impact of temperature change with sediments depth (i.e., the sediment geothermal gradient). Temperature has been implicated as having a significant effect on the potential rates of biogeochemical processes in deeply-buried sediments

---

* Tel.: +1 757 683 4930.
E-mail address: dburdige@odu.edu.

0012-821X/$ – see front matter © 2011 Elsevier B.V. All rights reserved.
doi:10.1016/j.epsl.2011.09.043

(Wellsbury et al., 1997), and as I will show, should play a major role in shaping not only the depth distribution of these processes, but also the overall biogeochemistry of the sediments.

The goal of this paper is to examine the effect of temperature on biogeochemical processes in deeply-buried sediments, using a coupled non-linear reactive-transport model. The results of this study provide a simple straight-forward explanation for the linear sulfate gradients commonly seen in many continental margin sediments (Borowski et al., 1999; Dickens, 2001; Hensen et al., 2003; Niewöhner et al., 1998; and others), and will also allow me to examine the mechanistic linkages between linear sulfate profiles, microbial processes in deeply-buried sediments, and the formation of gas hydrate deposits.

2. Organic matter remineralization in sediments and the effects of temperature on remineralization

Organic matter deposited in sediments is very heterogeneous in composition, and its reactivity is controlled both by its composition and structure as well as factors such as physical protection and, in some cases, electron acceptor availability (Burdige, 2007; Hedges and Keil, 1995; Hedges et al., 2000). Parameterizing this reactivity in reactive transport models is therefore a topic of some interest (Boudreau and Ruddick, 1991; Middelburg, 1989; Wallmann et al., 2006). Both qualitatively (Cowie and Hedges, 1994) and quantitatively (Middelburg, 1989) it has been shown that organic matter reactivity decreases with increasing age or sediment burial, in part because more reactive organic matter is preferentially remineralized, leaving behind less reactive organic matter for subsequent decomposition. The multi-G model (Westrich and Berner, 1984) quantifies this reactivity by assuming there are discrete organic matter fractions with decreasing rate constants for degradation. Laboratory studies of sediment organic matter remineralization have been be successfully analyzed with this approach (Burdige, 1991; Westrich and Berner, 1984), and variants of the multi-G model have also been used in many studies of shallow sediments (less than a few meters sediment depth[1]) in coastal, continental margin and deep-sea settings (for a review, see Burdige, 2006).

Continuous models of organic matter reactivity, such as the Middelburg power model (Middelburg, 1989), are based on empirical observations which show that there is a continuous decrease in the reactivity of bulk organic matter (as expressed by the first order rate constant for decomposition) as this material ages during transport to the sediments plus burial in the sediments. The multi-G model and the power model are not, however, necessarily mutually exclusive. This is because in the multi-G model the model-defined fractions of organic matter that are remineralized on early diagenetic time scales in different shallow sediments show a similar decrease in reactivity as one moves from coastal to deep sea sediments, consistent with the apparent aging of the material along this same environmental gradient (Burdige, 2006; Middelburg, 1989).

At the same time, an examination of the data used in the Middelburg (Middelburg, 1989) power model shows that as the age of the material undergoing remineralization decreases so does, in general, the temperature at which this remineralization occurs. One moves from "fresh" organic matter being degraded at temperatures of up to 15–25 °C, to more refractory organic matter being degraded in deep sea sediments at temperatures of ~2 °C. As a result, some of the observed trend of decreasing reactivity with increasing age may be related to this decreasing temperature. However, given the relatively "small" temperature change here (maximum of ~20 °C) versus the much larger (multi-order of magnitude) changes in organic matter reactivity, this temperature effect is likely to be quite small. Nevertheless, this consideration of temperature effects does point out that both the power model and multi-G models do not account for how the reactivity of a given "type" of organic matter may change as it undergoes deep burial (tens to several hundreds of meters) and heating by the natural geothermal gradient.

The importance of temperature on remineralization processes in deeply-buried marine sediments can be seen in the following simple calculation. Assuming that the temperature dependence of the rate constant (k_T) of a biogeochemical reaction can be described by the Arrhenius equation,

$$k_T = Ae^{-Ea/RT} \tag{1}$$

results from nearshore, coastal sediments suggest that the activation energy (Ea) for organic matter remineralization (primarily sulfate reduction) ranges from ~50 to 130 kJ mol^{-1} (Aller, 1980; Hu, 2007; Klump and Martens, 1989; Middelburg et al., 1996; Robador et al., 2009; Weston and Joye, 2005; Westrich and Berner, 1988). Furthermore, results of some of these studies (Middelburg et al., 1996; Westrich and Berner, 1988) also show that Ea values increase with decreasing organic matter "reactivity."

As discussed above, more refractory organic matter is generally deposited in outer continental margin and deep-sea (versus nearshore) sediments (Cowie and Hedges, 1994; Middelburg, 1989). This then suggests that the Ea values discussed above are likely lower limits for the Ea values of organic matter found in the types of deeply-buried outer continental margin sediments being examined in this study. Similarly, the activation energy for hydrocarbon generation from kerogen is ~200–250 kJ mol^{-1} (Hunt, 1996; Rullkötter, 2006), consistent with the observation that the activation energy for organic matter remineralization increases with decreasing reactivity. However given the many differences between microbially-mediated organic matter remineralization and abiotic hydrocarbon formation during organic matter catagenesis, it is obvious that some care must be taken in the interpretation of this comparison.

Given a range for the geothermal gradient in marine sediments of ~0.02 to 0.06 °C m^{-1} (Bohrmann and Torres, 2006), a temperature increase of ~20–30 °C is generally observed in the upper several hundred meters of marine sediment. With the activation energies listed above, this implies that rates of biogeochemical reactions in marine sediments can be expected to increase by up to several hundred-fold with deep burial. The incorporation of this temperature/depth dependence of reaction rates has not, to my knowledge, been included in reactive-transport models of sediment diagenesis in deeply-buried marine sediments.

Although other studies use a more sophisticated approach to incorporate thermodynamic controls on the kinetic parameters for microbial processes in nature (Jin and Bethke, 2005) I believe that the approach taken here is adequate for the goals of this study. Thus in the remainder of the discussion here I will use Eq. (1) to parameterize the temperature dependence of organic matter remineralization in deeply-buried sediments.

3. Methods

3.1. Reactive-transport model of biogeochemical processes in deeply buried marine sediments

The model used here consists of a set of coupled non-linear differential equations describing the depth-distribution of pore water sulfate (S) and methane (M) and solid phase (particulate) organic matter that has the "potential" to undergo remineralization (G). The relevant biogeochemical reactions considered in the model (and the constituents they affect) are: sulfate reduction coupled to organic matter remineralization/oxidation (G, S); methanogenesis (methane

---

[1] Throughout this paper, "shallow" is used to define or describe sediment depths relative to the sediment surface, rather than the water column depth at which the sediment is found.

production from organic matter; G, M), and anaerobic oxidation of methane (S, M). These reactions can be expressed as,

$$2CH_2O + SO_4^{2-} \rightarrow 2HCO_3^- + H_2S \tag{2a}$$

$$2CH_2O \rightarrow CH_4 + CO_2 \tag{2b}$$

$$CH_4 + SO_4^{2-} \rightarrow HCO_3^- + HS^- + H_2O. \tag{2c}$$

For simplicity I have assumed that the OM undergoing oxidation (i.e., CH_2O) has an oxidation state of 0, although in actuality it may be slightly more reduced (Burdige, 2006). The kinetics of sulfate reduction, methanogenesis and anaerobic oxidation of methane (AOM) are modeled as has been done previously (e.g., Burdige and Komada, 2011; Martens et al., 1998), modified to take into account changes in the rate constant of organic matter remineralization with increasing temperature/sediment burial (see below). Additional general details about these types of reactive-transport models can be found in the literature (Boudreau, 2000; Burdige, 2006).

For pore water sulfate, the differential equation used in the model is:

$$\frac{\partial S}{\partial t} = \frac{1}{\varphi}\frac{\partial}{\partial z}\left(\varphi D_s \frac{\partial S}{\partial z}\right) - \frac{1}{\varphi}\frac{\partial}{\partial z}(\varphi \nu S) - \frac{k_T L_1 \Im G S}{K_m + S} - k_{aom} S M \tag{3}$$

including (in order) the following processes on the right side of the equation: diffusion, advection, sulfate reduction and AOM. The analogous equation for pore water methane is:

$$\frac{\partial M}{\partial t} = \frac{1}{\varphi}\frac{\partial}{\partial z}\left(\varphi D_m \frac{\partial M}{\partial z}\right) - \frac{1}{\varphi}\frac{\partial}{\partial z}(\varphi \nu M) + f_S k_T L_2 \Im G - k_{aom} S M \tag{4}$$

and includes diffusion, advection, methanogenesis and AOM. Finally, the equation for sediment organic carbon is:

$$\frac{\partial G}{\partial t} = -\frac{1}{(1-\varphi)}\frac{\partial}{\partial z}(\omega(1-\varphi)G) - \frac{k_T G S}{K_m + S} - f_S k_T G \tag{5}$$

and includes advection driven by sedimentation, sulfate reduction and methanogenesis. Note that because of the relatively large depth-scale of these systems (i.e., 10s to 100s of meters), benthic processes that impact transport and biogeochemical reactions in the upper 10s of centimeters of sediment, or less, (e.g., bioturbation and bioirrigation) can be safely ignored.

The variables used in these equations are as follows: t = time; z = depth (positive downwards); ν = pore water advection; ω = sediment accumulation; k_T = the temperature-dependent first order rate constant for organic matter degradation, defined in Eq. (1); L_1 = moles of sulfate reduced per mole of OM oxidized and L_2 = moles of methane produced per mole of OM oxidized. Here these values both equal 1/2 (see Eqs. (2a) and (2b)). K_m is the half-saturation constant for bacterial sulfate reduction; a value of 0.5 mM was used in all calculations. This value is roughly in the middle of the range of values determined with sediment incubation studies (Boudreau and Westrich, 1984; Roychoudhury et al., 1998) or used in previous reactive-transport models (Dale et al., 2008). Model results are extremely insensitive to the choice of K_m values within this reported range (results not shown here). Porosity (φ) was assumed to decrease with depth, due to sediment compaction, according to,

$$\varphi = \varphi_\infty + (\varphi_o - \varphi_\infty)e^{-\alpha z} \tag{7}$$

where α is the porosity depth attenuation constant and the sub-scripts 'o' and '∞' refer to the sediment surface and some great depth in the sediments at which compaction ceases. Other formulations for the depth-dependence of porosity (both continuous and discontinuous functions) can easily be incorporated into the model equations and their numerical solution. I have also assumed steady-state compaction, i.e., φ is a function of depth but not time (see below for details). The parameter $\Im$ is used to convert dry sediment organic carbon concentrations (mg C g_{dw}^{-1}) to equivalent pore water concentrations (e.g., mM),

$$\Im = \frac{1-\varphi}{\varphi}\rho_{ds} \cdot \left(10^3/12\right) \tag{8}$$

where ρ_{ds} is the dry sediment density (Burdige, 2006). Since $\Im$ is a function of φ, and φ is a function of depth, $\Im$ is similarly depth-dependent.

The diffusion coefficients for sulfate and methane were corrected for sediment tortuosity (θ^2) using the equation,

$$D_i = \frac{D_i^o}{\theta^2} = \frac{D_i^o}{\varphi F} = D_i^o \varphi \tag{9}$$

where D_i^o is the temperature-dependent, free solution diffusion coefficient (see below), and $\theta^2 = \varphi F$ (Burdige, 2006). F, the so-called formation factor, was assumed to follow Archie's Law, or $F = \varphi^{-2}$ (Berner, 1980). Free solution diffusion coefficients were assumed to be a linear function of temperature

$$D_i^o = a_i + b_i T \tag{10}$$

where T is temperature (°C). The values of a_i and b_i for sulfate and methane were obtained by interpolating published diffusion coefficients (Schulz and Zabel, 2006).

Based on the temperature-dependence of diffusion coefficients, plus the depth-dependence of porosity, the derivative in the diffusive term in Eq. (3) is expanded as follows,

$$\begin{aligned}\frac{1}{\varphi}\frac{\partial}{\partial z}\left(\varphi D_s \frac{\partial S}{\partial z}\right) &= \frac{1}{\varphi}\frac{\partial}{\partial z}\left(\varphi^2 D_s^o \frac{\partial S}{\partial z}\right) = \frac{1}{\varphi}\left(2\varphi \frac{\partial \varphi}{\partial z} D_s^o \frac{\partial S}{\partial z} + \varphi^2 \frac{\partial D_s^o}{\partial z}\frac{\partial S}{\partial z} + \varphi^2 D_s^o \frac{\partial^2 S}{\partial z^2}\right) \\ &= 2D_s^o \frac{\partial \varphi}{\partial z}\frac{\partial S}{\partial z} + \varphi \frac{\partial D_s^o}{\partial z}\frac{\partial S}{\partial z} + \varphi D_s^o \frac{\partial^2 S}{\partial z^2}\end{aligned} \tag{11}$$

with the same also being true for methane (M) in Eq. (4). Based on Eq. (10) $\partial D_i^o/\partial z$ is given by,

$$\frac{\partial D_i^o}{\partial z} = \frac{\partial D_i^o}{\partial T}\frac{\partial T}{\partial z} = b_i G_T \tag{12}$$

where G_T is the geothermal gradient (°C m^{-1}).

In sediments where porosity decreases with depth, sediment burial (ω) and pore water advection (ν) are driven by sediment accumulation at the sediment surface and compaction with depth (Burdige, 2006; Meysman et al., 2005). A common assumption made in these cases is steady state compaction, i.e., $\partial\varphi/\partial z = 0$ (Berner, 1980). Here conservation of mass and pore water implies that the products $\varphi\nu$ and $(1-\varphi)\omega$ are constant with depth, despite the fact that their individual components (φ, ν and ω) vary with depth. Thus for solids, $(1-\varphi)\omega = (1-\varphi_\infty)\omega_\infty$, and the advective term in Eq. (5) can be re-written as,

$$\frac{1}{(1-\varphi)}\frac{\partial}{\partial z}(\omega(1-\varphi)G) = \frac{(1-\varphi_\infty)\omega_\infty}{(1-\varphi)}\frac{\partial G}{\partial z}. \tag{13}$$

Similarly, the pore water advective terms in either Eqs. (3) or (4) can be re-written as (again using sulfate as the example),

$$\frac{1}{\varphi}\frac{\partial}{\partial z}(\nu\varphi S) = \frac{\varphi_\infty \nu_\infty}{\varphi}\frac{\partial S}{\partial z} = \frac{\varphi_\infty \omega_\infty}{\varphi}\frac{\partial S}{\partial z} \tag{14}$$

since at the base of the compaction zone pore water advection and sedimentation occur at roughly the same rate, i.e., $\nu_\infty \approx \omega_\infty$, allowing for the substitution of ω_∞ for ν_∞.

In many gas hydrate-bearing sediments, though, the net pore water flow appears to be upwards (Davie and Buffett, 2003b; Egeberg and Dickens, 1999; Hensen and Wallmann, 2005), and pore water advection and sediment burial uncoupled from one another. In these sediments, net pore water advection results from downward advection due to sediment burial and upward pore water flow, and can be defined as (Luff and Wallmann, 2003),

$$\nu = \frac{(\varphi_\infty \omega_\infty + u_o \varphi_o)}{\varphi} \tag{15}$$

where u_o is the gross rate of pore water advection at the sediment surface. Since here the quantity $\nu\varphi$ is again independent of depth, the equivalent of Eq. (14) can be written as,

$$\frac{1}{\varphi}\frac{\partial}{\partial z}(\nu\varphi S) = \frac{(\varphi_\infty \omega_\infty + u_o \varphi_o)}{\varphi}\frac{\partial S}{\partial z}. \tag{16}$$

Notice that when $u_o = 0$ Eq. (16) is identical to Eq. (14). The causes of this upward advection are discussed further in Section 4.2.

The function f_S is an empirical "inhibition" function that goes from 0 to 1 as sulfate concentrations go to zero, providing a way to inhibit the occurrence of methanogenesis when sulfate is present. Several different forms of this inhibition function have been presented in the literature (e.g., Burdige and Komada, 2011; Martens et al., 1998) although all behave very similarly. Here, I have used the formulation,

$$f_S = \frac{10^{-5}}{10^{-5} + S} \tag{17}$$

which leads to the inhibition of methanogenesis ($f_S \rightarrow 0$) as sulfate increases above ~10^{-3} mM (Burdige and Komada, 2011).

3.2. Method of solution

Eqs. (3)–(5) represent a set of coupled, non-linear differential equations for which there is no analytical solution. The solution of these equations was obtained numerically using the Method of Lines technique with variable grid spacing (Boudreau, 1997; Schiesser, 1991). The spatial domain of the solution (defined here from 0 to L) was first sub-divided by n grid points, distributed such that the Δz_i value between grid points increased as depth increased (having a finer grid-spacing near the sediment–water interface allows one to more accurately represent concentration profiles and gradients in this region of the sediments where these parameters often show rapid changes). At each grid point, $\partial G/\partial z$ in Eq. (5) was approximated using a backwards difference approximation while the first and second space derivatives of sulfate and methane concentration in Eqs. (3) and (4) were approximated using centered, finite-difference approximations (Boudreau, 1997).

With this approach, Eqs. (3)–(5) are transformed from space- and time-dependent partial differential equations into a set ($3n$ total) of time-dependent ordinary differential equations (ODEs) valid at each of the n grid points. This set of coupled, non-linear ODEs was solved in MATLAB using the integration package *ode15s* (a copy of the complete MATLAB script is available from the author). The stiffness of this set of ODEs is well handled by this integration package.

Solving these equations using the Method of Lines actually results in a time-dependent solution to the three model equations (concentration versus depth versus time), although here only steady-state solutions are presented. The model was generally run forwards in time for ~100,000 kyr although a steady-state was reached after ~80,000 kyr.

For the upper boundary condition of the model (i.e., at $z = 0$), the concentrations of sulfate and methane were set to bottom water values (S_0 and M_0), and the concentration of organic carbon that has the potential to undergo remineralization (G^0) was specified at the sediment surface. At the lower boundary ($z = L$) it was assumed that $\partial S/\partial z$ and $\partial M/\partial z$ go to zero. Other model input parameters used here are listed in Table 1.

4. Model results and discussion

4.1. The effect of temperature

Fig. 1 presents model results illustrating the impact of temperature on organic matter remineralization in deeply-buried marine sediments. In these model calculations sulfate reduction was assumed to be the only remineralization process occurring in the sediments. Although this assumption is obviously not realistic, the results of these model runs nevertheless illustrate a key concept that subsequently will be elaborated upon using more realistic model simulations.

In these simulations k_T (2 °C) at the sediment surface was 10^{-7} kyr^{-1}. This rate constant is at least 3 orders of magnitude smaller than typical deep-sea sediment values (Middelburg, 1989), and as a result, when $Ea = 0$ kJ mol^{-1} (i.e., k_T is invariant with depth/temperature) essentially no remineralization of this organic matter occurs. However, as Ea increases, the importance of sub-surface remineralization increases, due to the increase of k_T with depth as a result of heating by the geothermal gradient. This then results in dramatic differences in pore water sulfate profiles and depth profiles of sulfate reduction rate. When, for example, $Ea = 200$ kJ mol^{-1}, the balance between k_T increasing with sediment depth as sediment temperature increases and the resulting depletion of pore water sulfate leads to the development of a well-defined sub-surface reaction zone.

In real marine sediments, however, if reactive organic matter still remains once sulfate is depleted, methanogenesis should occur (e.g., Claypool and Kaplan, 1974). In coastal or nearshore marine sediments where sulfate reduction and methanogenesis occur in the upper several meters (or less) of sediment, methanogenesis occurs immediately below the zone of sulfate reduction, once pore water sulfate is completely (or near completely) consumed (Martens and Berner, 1974; Reeburgh, 2007). In this case, the occurrence (depth distribution) of sulfate reduction and methanogenesis is primarily driven by the deposition (downward burial) of reactive organic matter (Claypool and Kaplan, 1974; Martens et al., 1998), since temperature changes over these sediment depth intervals are relatively small (less than a few degrees at most). The region in the sediments where sulfate concentrations go to zero is often referred to as the sulfate-methane transition zone (SMTZ), and it is generally a locus of AOM activity due to the upward diffusion of methane and the

Table 1
Input parameters used in the model simulations discussed in the text.

Parameter[a]	Fig. 1	Figs. 2 and 3	Fig. 4	Fig. 7	Units
G^0	4	4	4	4	mg C g_{dw}^{-1}
ω_∞	0.03	0.03	0.03	0.03	m kyr^{-1}
u_o	0	0	0	−0.03	m kyr^{-1}
G_T	0.03	0.03	0.03	0.03	°C m^{-1}
k_T (2 °C)	10^{-7}	10^{-7}	10^{-7}, 10^{-6}, 10^{-5}	10^{-7}	kyr^{-1}
k_{aom}[b]	–	10	10	10	mM^{-1} kyr^{-1}
Ea	0–200	200	200	200	kJ mol^{-1}
BWT	2	2	2	2	°C
φ_o	0.9	0.9	0.9	0.9	
φ_∞	0.65	0.65	0.65	0.65	
α	0.05	0.05	0.05	0.05	m^{-1}

[a] All model input parameters are defined in Section 3.1, as are the values of other parameters not shown here.

[b] This value is taken from Hensen and Wallmann (2005). Decreasing k_{aom} increases the curvature in sulfate profiles near the SMTZ, and spreads out the depth zone over which AOM occurs (results not shown here). These observations are most pronounced when k_{aom} is decreased from 10 to 1 (to 0.1) mM^{-1} kyr^{-1}, as opposed to decreasing it from 100 to 10 mM^{-1} kyr^{-1}. However, these changes in k_{aom} (with all other parameters held constant) result in no change (<1% difference) in the depth-integrated rate of AOM.

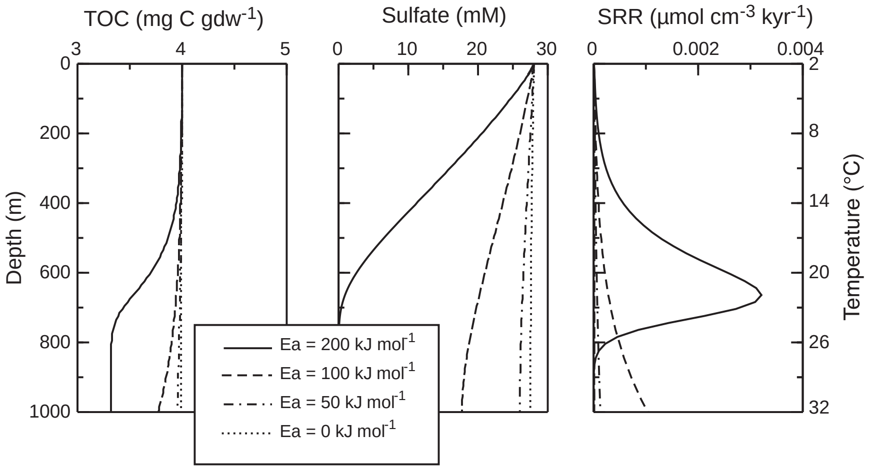

Fig. 1. Model-derived depth profiles of total organic carbon that has the potential to undergo remineralization (TOC), pore water sulfate concentration, and sulfate reduction rate (SRR) as a function of the activation energy of organic matter remineralization. In this and all other figures rates are expressed per cm^3 of total wet sediment. All other model input parameters are listed in Table 1 or discussed in Section 3.1. As discussed in the text, these model calculations do not allow for the occurrence of methanogenesis when reactive TOC remains at depth after complete pore water sulfate depletion.

downward diffusion of sulfate (e.g., Alperin and Hoehler, 2009; Dale et al., 2008).

In deeply buried sediments on the other hand, model results show that the occurrence of organic matter remineralization, and the reactivity of the organic matter itself, is further controlled by the geothermal gradient (G_T) and the *Ea* value for remineralization, in addition to the organic matter burial flux. For organic matter that is refractory at the sediment surface G_T and *Ea* define the increase with sediment depth in the reactivity of this material (regardless of the type of remineralization). If sulfate is able to diffuse downward to sediment depths where there has been this appreciable increase in organic matter reactivity, then bacterial sulfate reduction will oxidize this organic matter, and if reactive organic matter still remains after complete sulfate depletion, then methanogenesis will occur. In such a situation, as methane is produced it will diffuse upwards where it is consumed by microbes that mediate AOM. This shifts the SMTZ upwards and as this occurs the relative importance of sulfate reduction coupled to organic matter oxidation above the SMTZ decreases (since temperatures get lower as you move upward). With this, the relative importance of methanogenesis then increases in the deeper, warmer sediments. Under steady state conditions, the combined effect of this is a deep methanogenic reaction zone separated by a region of up to several hundred meters thick, in which methane diffuses upwards to be oxidized by downwardly diffusing sulfate.

This is illustrated in Figs. 2 and 3 in a model run ($Ea = 200$ kJ mol^{-1}) that includes methanogenesis and AOM. These results still show a deep zone of organic matter remineralization as in Fig. 1 although as noted above, methanogenesis is the terminal remineralization process here. The maximum rate of methanogenesis occurs at a sediment depth of ~900 m, more than 700 m below the SMTZ at ~130 m, and ~60% of the methanogenesis in these model sediments occurs between 720 and 960 m. At the same time, virtually all of the sulfate reduction occurs by AOM, with less than a few percent occurring through direct organic matter oxidation (Table 2). Increasing k_T (2 °C) 10- or 100-fold (to 10^{-6} and 10^{-5} kyr^{-1}) results in sediment profiles with near-identical general shapes, but which are shifted upwards: the SMTZ shifts from ~130 to 100 to 80 m, and the center of the zone of methane production moves from ~900 to 600 to 360 m (Fig. 4; also see Section 4.3 for a further discussion of the trends in this figure). The model profiles shown in Figs. 2–4 are broadly consistent with those observed across a wide range of continental margin sediments (Borowski et al., 1999; Dickens, 2001; Hensen and Wallmann, 2005; Niewöhner et al., 1998; Sivan et al., 2007), suggesting that this model provides a plausible first-order explanation for the factors controlling such pore water profiles in these settings (also see additional discussions Sections 4.2 and 4.4).

Based on these model results, organic matter that is refractory at sea floor temperatures is buried in sediments and not degraded by sulfate reducing bacteria above the SMTZ, but is degraded deeper in the sediments by methanogens. At first glance, such an observation appears to "violate" a fundamental tenet of sediment biogeochemistry, the concept of biogeochemical zonation (Claypool and Kaplan, 1974; Froelich et al., 1979). Based on this concept, the degradation of the same type of organic matter should occur by sulfate reduction before methanogenesis (i.e., higher up in the sediment column) since sulfate reduction yields a greater amount of free energy per mole of organic matter that is oxidized than does methanogenesis. While this type of separation/zonation is seen in shallow coastal sediments (e.g., Alperin et al., 1992; Dale et al., 2008; Martens et al., 1998), it does not occur this way in certain deeply-buried marine sediments. Here, increasing temperature (with increasing sediment burial) allows organic matter that is refractory at sea floor temperatures to bypass extensive remineralization by sulfate reduction in shallow sediments with lower temperatures, followed by remineralization in deeper sediments with higher temperatures.

4.2. Linear sulfate gradients

A linear least squares fit to the model sulfate data in Fig. 2A from 25 m below the sediment surface down to just above the SMTZ yields a line with a very high r^2 value ($=0.999$, see Fig. 3A). Model sulfate profiles shown in Fig. 4 or discussed in Table 2 also have similar high r^2 values (>0.998) in this general region of the sediments. There is, however, some curvature in these profiles, particularly near the sediment surface, due to the decrease in porosity with sediment depth, and its resulting decrease in the magnitude of the sulfate diffusion coefficient (see Eq. (9) and Lerman, 1977). This effect is most pronounced in the upper ~10–20 m of these profiles, since the porosity attenuation coefficient α used in Eq. (7) is 0.05 m^{-1}, implying that the *e*-folding depth for a porosity decrease is 20 m. Also, despite the subtle curvature in profiles such as that in Fig. 2A, a linear least square fit to all of the sulfate data from the sediment surface to the SMTZ yields a line with an r^2 value that is only slight diminished ($=0.996$) from that for the data in the sulfate reduction zone below 25 m. Similarly, the slopes for the two best-fit lines are virtually identical.

On depth scales of several 10s of meters not all continental margin sulfate profiles show this high degree of linearity (Borowski et al.,

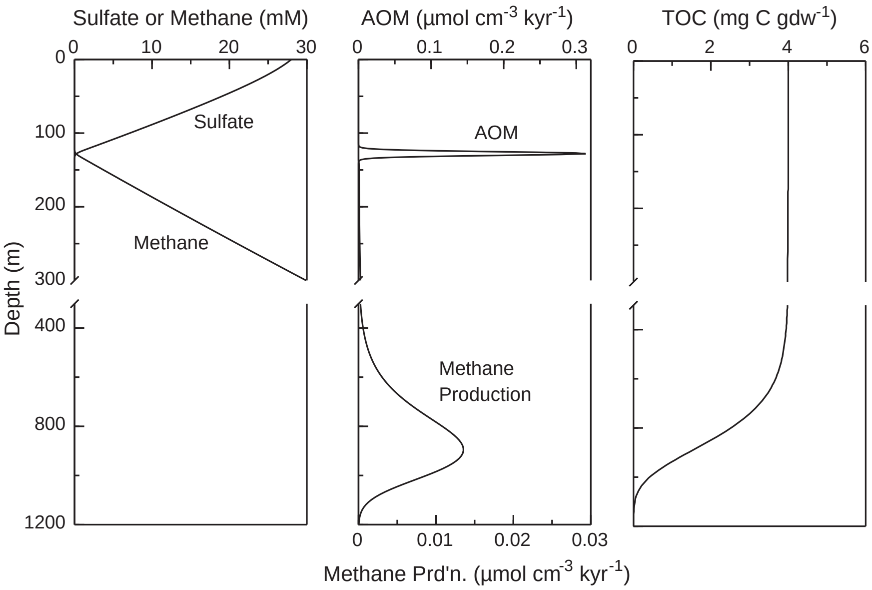

Fig. 2. Model-derived depth profiles of pore water sulfate and methane (left panel), AOM and methane production rates (center panel) and total organic carbon that has the potential to undergo remineralization (TOC; right panel). The activation energy (*Ea*) used in this calculation was 200 kJ mol^{-1} and all other model input parameters are either listed in Table 1 or discussed in Section 3.1. Note that this is model run E in Table 2.

1999), and some profiles show either smooth or “kinked” concave up profiles for reasons beside porosity variations. In particular, this may be due to non-steady state effects associated with large scale sediment slumping (slides) possibly in combination with changing deep methane fluxes (Hensen et al., 2003). Similarly, sulfate profiles may also show smooth or kinked concave down profiles. One possible explanation for these profiles is “high” rates of sulfate reduction coupled to organic matter oxidation near the sediment surface with lower rates of AOM at depth (Borowski et al., 1999).

To examine these latter types of profiles, I first note that model calculations presented so far assume there is only one type of refractory organic matter deposited in the sediments, and that this material becomes more reactive with depth due to increasing temperature. In addition, even with a value of k_T (2 °C) equal to 10^{-5} kyr^{-1} ($\equiv 10^{-8}$ yr^{-1}), this material is still several orders of magnitude less reactive than “typical” organic matter than undergoes remineralization in the upper few meters of most continental sediments (Middelburg, 1989; Wallmann et al., 2006).

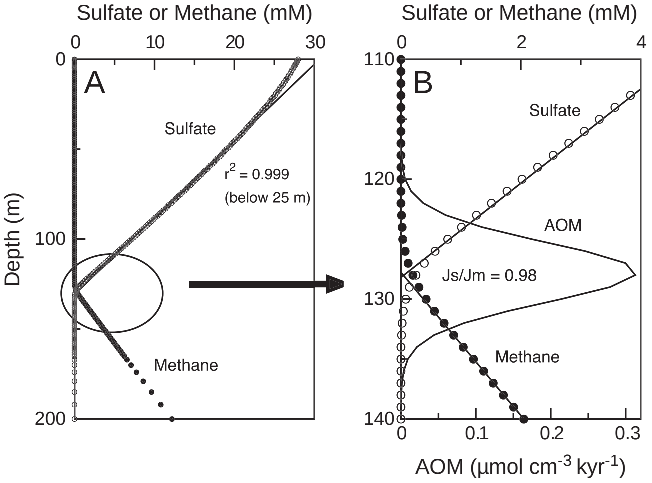

Fig. 3. (A) An expanded view of the model-derived sulfate and methane profiles shown in Fig. 2 (model run E in Table 2), illustrating the high degree of linearity of the sulfate profile from ~25 m below the sediment surface to just above the SMTZ. (B) An expanded view around the SMTZ of the model-derived sulfate and methane concentration and the AOM rate profiles shown in Fig. 2. The best-fit straight lines through the model data above and below the SMTZ were used to calculate the diffusive fluxes of sulfate and methane into the SMTZ. The ratio of these fluxes was ~1, consistent with the stoichiometry of AOM and emphasizing that virtually all sulfate reduction in the SMTZ occurs at the expense of AOM (also see Table 2).

Therefore in the set of calculations shown in Fig. 5 I have included a second model equation for a more reactive fraction of organic matter that degrades near the sediment surface. Both equations are based on Eq. (5), one for a reactive “G$_1$” fraction and the second for a refractory “G$_2$” fraction, each with different k_T (2 °C) and *Ea* values. Similarly, the equations for sulfate and methane now include terms for sulfate reduction and methanogenesis coupled to the remineralization of each of these two types of organic matter. For example, the sulfate equation in this 2-G model is now written as,

$$\frac{\partial S}{\partial t} = \frac{1}{\varphi}\frac{\partial}{\partial z}\left(\varphi D_s \frac{\partial S}{\partial z}\right) - \frac{1}{\varphi}\frac{\partial}{\partial z}(\varphi \nu S) - \frac{k_{T,1}L_1\Im G_1 S}{K_m + S} - \frac{k_{T,2}L_2\Im G_2 S}{K_m + S} - k_{aom}SM. \qquad (18)$$

In these calculations I have assumed that the G$_2$ organic matter has a $k_{T,2}$ (2 °C) value equal to 10^{-5} kyr^{-1} and an *Ea* of 200 kJ mol^{-1}. For the more reactive (G$_1$) organic matter fraction undergoing remineralization I assumed that the initial age of this material in surface continental margin sediments is 500–1000 yr (Middelburg, 1989; Wallmann et al., 2006), and using the Middelburg power model (Middelburg, 1989) this predicts a k value for this G$_1$ material (assumed to be equal to $k_{T,1}$ (2 °C) in the model) on the order of 10^{-4} yr^{-1} ($\equiv$0.1 kyr^{-1}). The *e*-folding depth for the remineralization of this material is roughly equal to ω/k, or ~1–10 m for typical continental margin sedimentation rates of ~0.1–1 m kyr^{-1}. Rate constants and *e*-folding depths such as these are often seen in many continental margin sediments (Boudreau, 1997; Wallmann et al., 2006). Based on arguments presented in Section 2, I have also assumed that this G$_1$ material has an *Ea* for remineralization of 100 kJ mol^{-1}, although given the relatively small *e*-folding depth for its remineralization, the temperature effect on remineralization is minimal. Also, shown in Fig. 5 is an additional set of calculations in which I have assumed $k_{T,1}$ (2 °C) for this G$_1$ fraction is ten times smaller (10^{-2} kyr^{-1}) with a corresponding 10-fold increase in the *e*-folding depth for its remineralization.

Table 2

A summary of model results illustrating the relationship between key model input parameters and biogeochemical zonation and processes in deeply-buried marine sediments.

Run[a]	k_T (2 °C) (kyr^{-1})	E_a ($\mathrm{kJ\ mol}^{-1}$)	G^0 ($\mathrm{mg\ g_{dw}^{-1}}$)	G_T ($\mathrm{°C\ m}^{-1}$)	z_{AOM}[b] (m)	z_{MP}[c] (m)	M_{max}[d] (mM)	Δz_{MA}[e] (m)	Δz_{MA}[f] (m)	Δz_{MA}[g] (m)	AOM:SRR ratio[h]	J_s:J_m ratio[i]
Changes in E_a												
A	5×10^{-7}	150	4	0.03	126	894	131	768	786	921	0.99	0.97
B	5×10^{-7}	200	4	0.03	108	694	115	586	601	696	1.00	0.97
C	1×10^{-6}	150	4	0.045	93	573	93	480	480	482	0.99	0.98
D	1×10^{-6}	200	4	0.045	84	447	79	363	364	370	0.99	0.98
Changes in k_T												
E[j]	1×10^{-7}	200	4	0.03	128	898	132	771	792	947	1.00	0.98
B	5×10^{-7}	200	4	0.03	108	694	115	586	601	696	0.99	0.97
F[k]	1×10^{-6}	200	4	0.03	100	614	106	514	526	594	0.99	0.97
H[k]	1×10^{-5}	200	4	0.03	78	356	68	278	282	299	0.96	0.97
C	1×10^{-6}	150	4	0.045	93	573	93	480	480	482	0.99	0.98
I	1×10^{-5}	150	4	0.045	76	331	60	255	256	256	0.96	0.98
Changes in G_T												
F	1×10^{-6}	200	4	0.03	100	614	106	514	526	594	0.99	0.97
D	1×10^{-6}	200	4	0.045	84	447	79	363	364	370	0.99	0.98
J	1×10^{-6}	150	4	0.03	114	794	121	680	692	773	0.99	0.97
C	1×10^{-6}	150	4	0.045	93	573	93	480	480	482	1.00	0.98
Change in TOC loading												
C	1×10^{-6}	150	4	0.045	93	573	93	480	480	482	0.99	0.98
K	1×10^{-6}	150	8	0.045	50	573	204	523	527	570	1.00	0.98
2-G models												
H[l]	1×10^{-5}	200	4	0.03	78	356	69	278	282	299	0.96	0.97
L	(G_1) 0.01	100	8	0.03	63	356	72	293	285	254	0.27	0.96
	(G_2) 1×10^{-5}	200	4									
M	(G_1) 0.01	100	6	0.03	47	356	74	309	287	196	0.39	0.93
	(G_2) 1×10^{-5}	200	6									
N	(G_1) 0.01	100	4	0.03	39	356	155	317	320	340	0.56	0.93
	(G_2) 1×10^{-5}	200	8									
O	(G_1) 0.1	100	8	0.03	77	356	69	280	283	294	0.23	0.97
	(G_2) 1×10^{-5}	200	4									
P	(G_1) 0.1	100	4	0.03	42	356	154	314	319	366	0.53	0.93
	(G_2) 1×10^{-5}	200	8									

[a] All other model input parameters used in these model runs were those used for model run E shown in Fig. 2. Also note that some model runs are listed multiple times (under different sub-sections of this table) to illustrate the trends being presented here.

[b] z_{AOM} is the depth at which the maximum rate of AOM occurs, determined by direct examination of model results (depth profiles of AOM).

[c] z_{MP} is the depth of the maximum methane production rate, determined by direct examination of model results (depth profiles of methane production).

[d] M_{max} is the maximum methane concentration, determined by direct examination of model results (depth profiles of methane concentrations).

[e] Based on direct model-derived values of z_{MP} and z_{AOM} listed here (i.e., $\Delta z_{\mathrm{MA}} = z_{\mathrm{MP}} - z_{\mathrm{AOM}}$).

[f] Determined with Eq. (21a).

[g] Determined with Eq. (21b).

[h] The depth-integrated rate of AOM divided by the depth-integrated rate of total sulfate reduction, defined as:

$$\int \left(k_{aom} SM \right) \mathrm{d}z \Big/ \int \left(\frac{k_T L_1 \Im G S}{K_m + S} + k_{aom} SM \right) dz.$$

Both integrals were solved by trapezoidal approximations using numerical model solutions and model input parameters in Tables 1 and 2.

[i] The diffusive flux of sulfate into the SMTZ (Js) divided by the diffusive flux of methane into the SMTZ (Jm). Concentration gradients were determined by linear least squares fitting of the sulfate or methane data immediately above or below the SMTZ (defined here by zAOM), respectively, before obvious curvature was seen in the model data within the SMTZ (see Section 4.2 for details).

[j] These model results are shown in Figs. 2–4.

[k] These model results are shown in Fig. 4.

[l] This model result is listed here for comparison since the organic matter undergoing remineralization in this 1-G model run has the same characteristics as the G2 fraction in these 2-G model runs.

As seen in Fig. 5, when the amount of G_1 organic matter is greater than that of the G_2 material (model runs L and O in this figure) the model sulfate profile is concave down, roughly over the depth range in which the G_1 material is remineralized. When the amount of refractory G_2 material is greater than the reactive G_1 material the sulfate profiles are highly linear over essentially the complete sulfate reduction zone (e.g., model run N), including here the shallow portion of the sediments where sulfate reduction coupled to organic matter oxidation is occurring.

In general, the ability to detect curvature near the sediment surface in pore water sulfate profiles from cores that may extend over several 100 m requires collection of pore water samples with the proper resolution to distinguish meter-scale features near the sediment surface. Low sample density (compared to that in the model runs presented here) plays a role in possibly obscuring any curvature near the sediment surface in real sulfate profiles in deeply-buried sediments, as does pore water sampling and/or analytical errors or uncertainties (Burdige and Komada, 2011). Similar factors may also impact the ability to detect subtle curvature in sulfate profiles over the larger depth scale of the total zone of sulfate reduction (e.g., see Fig. 4 or model runs O or P in Fig. 5).

Model results similarly predict curvature in sulfate profiles just above the zero sulfate concentration in the STMZ where AOM occurs (e.g., see Fig. 3). The concave-down nature of the sulfate model profiles

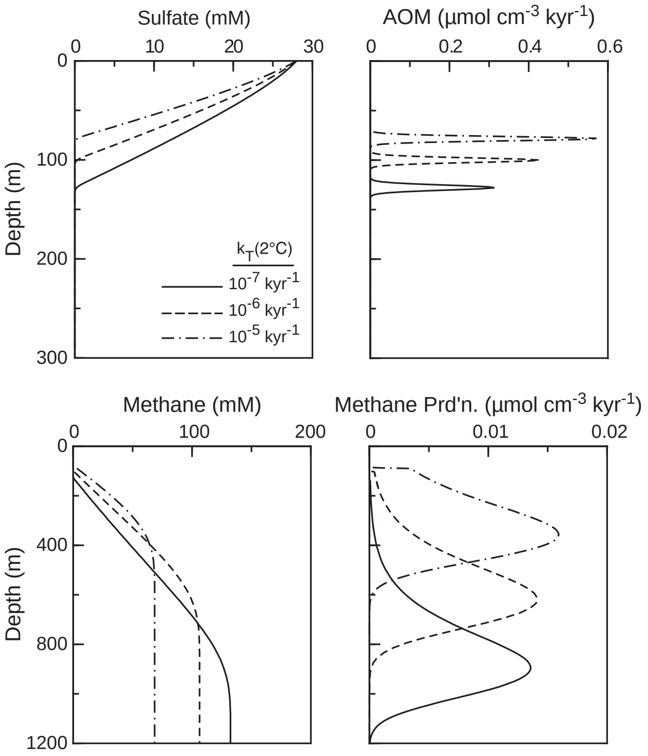

Fig. 4. Model-derived depth profiles of pore water sulfate and methane concentrations, and rates of AOM and methane production for three different k_T (2 °C) values (10^{-7}, 10^{-6} and 10^{-5} kyr^{-1}; model runs E, F, and H respectively, in Table 2). All other model input parameters are listed in Table 1 or discussed in Section 3.1. Note the different depth scales for the panels in the top row versus the bottom row.

near the SMTZ (due to downward diffusion and sulfate consumption by AOM) is consistent with the analogous concave-up methane profiles (due to upward diffusion and consumption by AOM), seen both in model runs here and in methane profiles from coastal sediments (e.g., Reeburgh, 2007). An examination of field data from deeply-buried sediments (Borowski et al., 1999) does not provide strong evidence for curvature in sulfate profiles in the SMTZ, and factors similar to those described above that can obscure curvature in sulfate profiles near the sediment surface may play a role here as well.

Overall then, what is often seen in many continental margin sediments are linear sulfate profiles roughly from the sediment surface to the SMTZ (Borowski et al., 1996, 1999; Dickens, 2001; Hensen et al., 2003; Niewöhner et al., 1998). Such profiles occur on depth scales of several meters to >100 m (i.e., the depth of the SMTZ), as is seen in the model profiles shown here. A "traditional" view of such profiles is that sulfate diffuses through the upper sediments with little or no apparent sulfate reduction occurring at the expense of sediment organic matter oxidation until the SMTZ, where sulfate is then used in AOM. Consistent with this explanation are the results in Table 2 for the 1-G model runs which show that here less than ~5% of the total sulfate reduction occurs at the direct expense of organic matter oxidation; the remaining >95% occurs via AOM.

In contrast though are the 2-G model runs in Fig. 5 where a significant fraction of the sulfate reduction does not occur by AOM, and some sulfate reduction coupled to organic matter oxidation also occurs in regions of the sediments where the profiles are linear. Here linearity in pore water profiles ultimately results from a region in the sediments in which diffusion alone occurs, although the location of the linear region does not identically match the region in the sediments in which no in situ reactions occur. Similar conclusions were also reached in studies of sulfate reduction and AOM in shallow (<5 m) sediments in Santa Monica Basin in the California Borderlands region (Burdige and Komada, 2011). An important finding that comes from both sets of observations is that the development of a sub-surface reaction zone isolated from surface sediment processes plays a crucial role in the occurrence of linear sulfate profiles seen over wide a range of depth scales in both inner and outer continental margin sediments, even when the majority of the sulfate reduction in the sediments does not occur at the expense of AOM.

In Fig. 3B it can also be seen that the gradients of both sulfate and methane into the SMTZ are highly linear, and that the ratio of the downward diffusive flux of sulfate and the upward diffusive flux of methane into the SMTZ is essentially 1. For all of the 1-G model runs in Table 2 this ratio is 0.97–0.98, consistent with the stoichiometry of AOM (Eq. (2c)) and with the lack of organic matter oxidation through sulfate reduction at depth in these sediments. For the 2-G model runs this ratio appears to be very slightly, but consistently, lower (0.93) when the depth of the SMTZ (as expressed by z_{AOM}) is shallower than ~50 m. The reasons for this are not clear, although effects due to porosity variations in shallow sediments may play a role.

In the literature linear sulfate gradients are often taken as indirect indicators of the occurrence of methane gas hydrates (Borowski et al., 1999; Davie and Buffett, 2003a). While this can be the case (see Section 4.4) the results in this section also demonstrate that this may not always the case. Furthermore, in the model used here the observed linear sulfate gradients are linked to in situ methane production by methanogenesis which is driven, albeit on extremely long time scales,

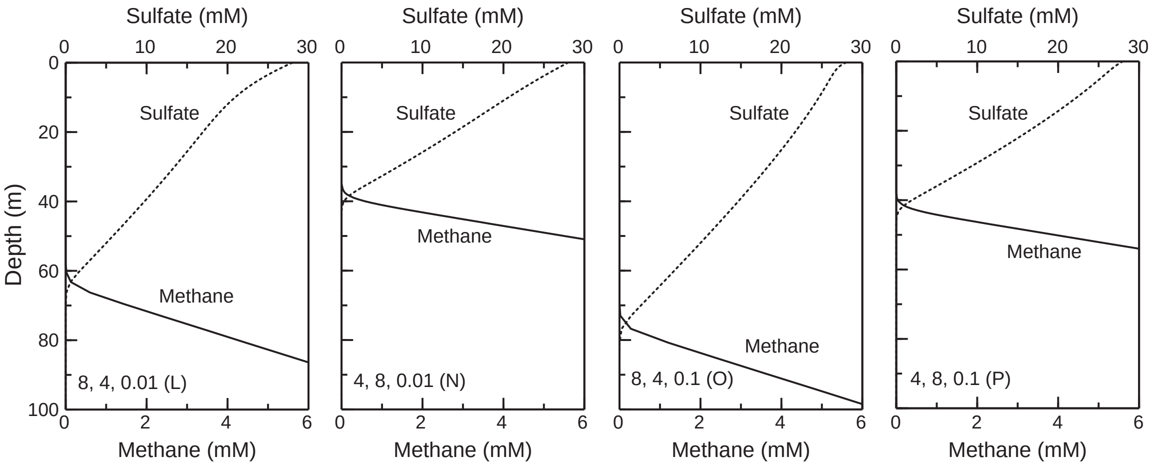

Fig. 5. Model-derived depth profiles of pore water sulfate and methane concentrations for model runs using the 2-G model. The three numbers in the bottom left corner of each panel are G_1^0, G_2^0 (both mg C g_{dw}^{-1}), and $k_{T,1}$ (2 °C) (kyr^{-1}) for that model run, The letter in parentheses is the designator of the model run in Table 2. In all model runs shown here $k_{T,2}$ (2 °C) = 1×10^{-5} kyr^{-1}, and all other model input parameters are listed in Table 1.

by surface organic carbon fluxes and organic matter burial. However in addition to dissolved methane produced by in situ methanogenesis, deeply-buried marine sediments can also contain "ancient" biogenic methane derived from older (and deeper) gas deposits (Bohrmann and Torres, 2006; Davie and Buffett, 2003b; Fehn et al., 2000; Paull et al., 1994) or thermogenic methane produced by abiotic catagenic processes (Bohrmann and Torres, 2006; Roussel et al., 2008). Catagenesis, though, only becomes significant at temperatures greater than ~50 °C (Hunt, 1996), and therefore for typical geothermal gradients in continental margin, or open ocean, sediments (i.e., ~0.03–0.04 °C m^{-1}) thermogenic methane production will only become important at sediment depths greater than at least ~1–1.5 km. Thus in the model simulations presented here, I do not consider thermogenic methane production, although in future work with this model it may be important to also consider this type of methane production. Questions about the sources of the methane that lead to linear sulfate and methane gradients will be re-examined in Section 4.4.

In coastal or inner continental shelf settings where the depth of SMTZ is on the order of only a few meters or less linear sulfate gradients are also linked to AOM in sediments (Berelson et al., 2005; Jørgensen and Parkes, 2010) although here the source of the methane does not always appear to be in situ methanogenesis. Instead, the methane may have an "external" source, which might include geologic hydrocarbon reservoirs derived from ancient source rocks, or gas hydrate deposits that ultimately derive from deeper gas deposits (Burdige and Komada, 2011). Elucidating the relationships between such similar linear sulfate profiles in shallow sediments and more deeply-buried sediments will require further field and modeling studies.

4.3. Controls on the depth zonation of biogeochemical processes in deeply buried sediments

The trends in Fig. 4 are part of a broader set of observations summarized in Table 2 which illustrate how key model input parameters impact biogeochemical processes in deeply-buried sediments. For the 1-G model results, increasing *Ea*, k_T (2 °C), or G_T all result in organic matter becoming more reactive at shallower depths, and this results in a decrease of the depth of maximum methane production (z_{MP}), an increase in the pore water methane gradient, and a decrease in the maximum methane concentration (M_{max}) seen at depth in the sediments. Since the upward flux of methane drives the observed AOM in the model results, these observed trends in methane profiles result in a general increase in the amount of AOM, which is evidenced by a shallowing of the depth at which the maximum rate of AOM occurs (z_{AOM}), an increase in the maximum rate of AOM at z_{AOM}, and an increase (steepening) in the pore water sulfate gradient.

In contrast to these trends, an increase in carbon loading has no impact on z_{MP} (which is controlled by *Ea*, G_T and k_T (2 °C)), but does increase the maximum rate of methanogenesis and the value of M_{max}. This then increases the pore water methane gradient, and hence causes a decrease in z_{AOM}. Similar trends are also seen when comparing the 2-G model results with run H from the 1-G models, since G_T is the same in all of these cases and the *Ea* and k_T (2 °C) for the organic matter in run H is the same as that for the G_2 organic matter in the 2-G model runs. The factors controlling the depth of z_{AOM} in the 2-G model runs are a bit more complex, since this depth depends on both the upward flux of methane (driven by the remineralization of the G_2 organic matter at depth), as well as consumption of sulfate in the shallow sediments associated with the remineralization of G_1 organic matter by sulfate reduction.

In all but the carbon loading scenario, changes in z_{AOM} and z_{MP} track one another, although they do not change equally, and their difference ($\Delta z_{MA} \equiv z_{MP} - z_{AOM}$) becomes smaller as each depth shallows. Given that the "cause and effect" amongst all of these quantities (e.g., z_{AOM}, z_{MP}, and M_{max}) is not necessarily straight-forward, the following simple calculation can be used to explore these trends in z_{AOM} and z_{MP}.

The explanation starts with the conceptual model in Fig. 6, which assumes that there is a linear sulfate gradient from the sediment surface to the SMTZ, and that we can use z_{AOM} to define the depth of the SMTZ. I similarly assume there is a linear methane gradient from the SMTZ to z_{MP} and that the methane concentration at z_{MP} is M_{max}. While these assumptions are not entirely correct, an examination of Figs. 2–5 suggests that they are nevertheless fairly reasonable.

At the SMTZ the upward flux of methane (J_M) balances the downward flux of sulfate (J_S), i.e., $J_M = -J_S$, and,

$$\varphi D_s \frac{dS}{dz} = -\varphi D_m \frac{dM}{dz}. \tag{19}$$

Based on the assumptions above, the two derivatives can be approximated as,

$$\frac{dS}{dz} \approx \frac{0 - S_o}{z_{AOM} - 0} \tag{20a}$$

$$\frac{dM}{dz} \approx \frac{M_{max} - 0}{z_{MP} - z_{AOM}} \tag{20b}$$

(recall S_0 is the bottom water sulfate concentration). Applying Eqs. (20a) and (20b) to Eq. (19) leads to the following two equations for Δz_{MA},

$$\Delta z_{MA} = z_{MP} \frac{1}{1+\gamma} \tag{21a}$$

$$\Delta z_{MA} = z_{AOM} \frac{1}{\gamma} \tag{21b}$$

where

$$\gamma = \frac{D_s}{D_m} \frac{S_o}{M_{max}}. \tag{22}$$

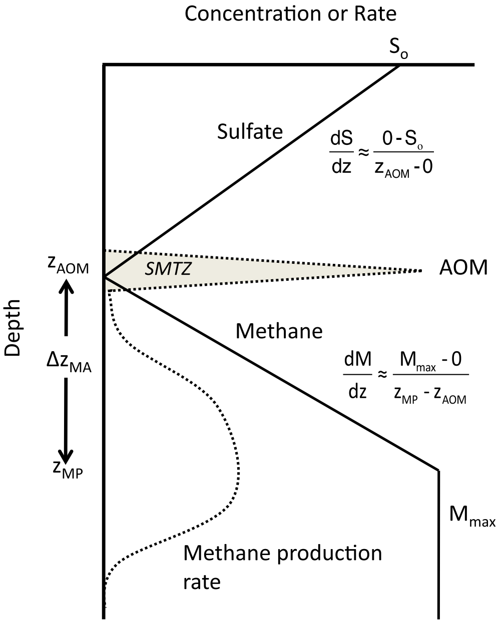

Fig. 6. A conceptual model illustrating the approximate relationship between the depth zonation of AOM and methane production in deeply-buried sediments. The symbols used here are defined in the text (see Section 4.3).

For a given set of parameters, the results in Table 2 show that in general, $M_{\max}$ decreases as z_{MP} or z_{AOM} decrease. Since all of the other terms on the right hand side of Eq. (22) are essentially constant, this implies that γ will similarly increase. Furthermore, because γ is a positive number, both $\frac{1}{\gamma}$ and $\frac{1}{1+\gamma}$ will then decrease as either z_{MP} or z_{AOM} decrease (become shallower). As a result, Δz_{MA} will therefore decrease as either depth decreases, but by a lesser amount.

Not only does this qualitatively explain the trends in Δz_{MA} based directly on the model results, but values of Δz_{MA} determined with either Eqs. (21a) or (21b) agree well with these values of Δz_{MA} obtained directly from model results. This observation also appears to be roughly true for both the 1-G and 2-G model results. For the 2-G model runs this suggests that the assumption upon which Fig. 6, and ultimately Eqs. (21a) and (21b), are based are not significantly impacted by organic matter remineralization processes occurring near the sediment surface.

The depth of the SMTZ ($\approx z_{\mathrm{AOM}}$) is itself largely controlled by the upward methane flux J_{M}, and a re-examination of Eqs. (16) and (17) shows that there is roughly an inverse relationship between z_{AOM} and J_{M} (Borowski et al., 1996):

$$z_{AOM} \approx \frac{-\varphi D_s S_o}{J_M}. \tag{23}$$

As discussed above, the magnitude of J_{M} is controlled by parameters that ultimately control the depth distribution and magnitude of methane production in the deep sediments.

4.4. Pore water advection in deeply-buried sediments

In many deeply-buried sediments, especially those associated with methane gas hydrates, the net pore water flow appears to be upwards (Davie and Buffett, 2003b; Egeberg and Dickens, 1999; Hensen and Wallmann, 2005). The causes of this upward advection include thermally-driven (geothermal) fluid flow, subduction-driven fluid expulsion in accretionary prism sediments, or nonsteady or nonuniform compaction of sediments that results in pore water overpressure (Buffett and Archer, 2004). In a modeling study of methane gas hydrate distribution in marine sediments, estimates of the global hydrate inventory were shown to be fairly sensitive to the rate of this fluid flow (Buffett and Archer, 2004).

Model results that include upward advection are shown in Fig. 7. The model parameters used here are identical to those used in the model run in Fig. 2, with the exception that here gross pore water advection is upwards ($u_o = -0.03$ m kyr^{-1}) as is net pore water advection (ν ranges from -0.008 to -0.011 m kyr^{-1}). In contrast, ν ranges from $+0.03$ to $+0.021$ m kyr^{-1} in Fig. 2 where pore water advection is downward and driven solely by sediment accumulation and compaction. The inclusion of upward advection shifts the SMTZ from ~130 m to ~40 m (see similar model results in Hensen and Wallmann, 2005), and also appears to produce sulfate profiles that are slightly more linear (i.e., there is less curvature in the profile in Fig. 7 near the sediment surface as compared to Fig. 2). However, the depth distribution of methane production is unchanged by upward advection, since the rate of methanogenesis is controlled by Ea, k_T (2 °C), and G_T, all of which were the same in both sets of model runs.

In these calculations with upward advection, the ratio of the downward diffusive sulfate flux to the upward diffusive methane flux at the SMTZ is 0.95, only slightly lower than it is for the model runs in Table 2. This occurs despite the presence of upward pore water advection augmenting diffusive methane transport into the SMTZ. For the advection rate used here a Peclet number analysis (Boudreau, 1997) over the length scale of solute transport into the SMTZ demonstrates the predominance of diffusive over advective transport into the SMTZ. For this reason we would therefore not expect this diffusive flux ratio to be significantly impacted by pore water advection of this magnitude.

4.5. Application to methane gas hydrate-containing sediments

In certain deeply-buried sediments, pore water methane concentrations approach in situ saturation values either due to in situ methanogenesis and/or methane input from deeper sediments. When methane saturation is reached, methane gas hydrates can form (Bohrmann and Torres, 2006). The depths where gas hydrates form will depend on the sediment depth at which the pore waters become saturated with methane and the lower boundary of the gas hydrate stability zone (GHSZ). This latter boundary depends on sediment temperature (controlled by the geothermal gradient), the in situ sediment hydrostatic pressure, and where these properties fall on the pressure vs. temperature stability fields for free gas or gas hydrate in equilibrium with dissolved methane (Bohrmann and Torres, 2006; Davie et al., 2004).

This last set of model calculations takes into account methane removal from pore waters (into either free methane gas or methane gas hydrates), to examine its relationship to the temperature-dependent remineralization processes discussed here. The results of these calculations will be compared with field data from the Blake Ridge on the southeast US continental margin, collected during ODP Leg 164 (Borowski, 2004; Dickens, 2001; Dickens et al., 1997; Paull et al., 1996, 2000; Ruppel, 1997). The sediments here are in water depths of ~2800 m, and contain gas hydrate below sediment depths of ~190 m. The lower boundary of the GHSZ in these sediments is ~450 m. Rate measurements suggest the occurrence of methanogenesis in the GHSZ (Wellsbury et al., 1997), and δ^{13}C and δD values of the methane found in the gas hydrates indicate that the gas is primarily of biogenic origin (Borowski et al., 1997; Hoehler et al., 2000). However, there is still uncertainty as to whether the methane found in the hydrates was produced by in situ methanogenesis in the GHSZ, or has migrated upward from deeper, and older, gas deposits (Borowski, 2004; Fehn et al., 2000; Paull et al., 1994; Wallmann et al., 2006).

To carry out these model calculations, the diagenetic equation for pore water methane (Eq. (4)) was modified to take into account methane removal into either gas hydrate or free gas, as:

$$\frac{\partial M}{\partial t} = \frac{1}{\varphi}\frac{\partial}{\partial z}\left(\varphi D_m \frac{\partial M}{\partial z}\right) - \frac{1}{\varphi}\frac{\partial}{\partial z}(\varphi \nu M) + f_S k_T L_2 \Im G - k_{aom} SM - k_{mr}\left(M - M_{eq}\right). \tag{24}$$

In the new term added to this equation, M_{eq} is the depth-dependent methane solubility concentration, which varies with sediment depth due to bottom water temperature, the sediment geothermal gradient, and water column depth (i.e., hydrostatic pressure). M_{eq} was calculated as outlined in Davie et al. (2004). The rate constant for methane removal, k_{mr}, has the following formulation (Torres et al., 2004),

$$k_{mr} = \begin{cases} 0, & \text{if} \quad M < M_{eq} \\ k_{mr}, & \text{if} \quad M \geq M_{eq}. \end{cases} \tag{25}$$

In the current modeling effort, I have not attempted to differentiate between methane removal from the pore waters into gas hydrate or into free gas, nor have I considered methane cycling around the base of the gas hydrate stability zone between methane in pore waters, gas hydrates, or the free gas phase (Hensen and Wallmann, 2005; Paull et al., 1994; Torres et al., 2004).

The results in Fig. 8 represent eyeball fits of the model to pore water sulfate and methane results from ODP Leg 164, site 994 on the Blake Ridge (Borowski et al., 2000). Wherever possible, reported literature values were used to constrain model input parameters (Table 3). However for some parameters, (e.g., Ea) this was not possible. These results appear to somewhat sensitive to the choice of u_o,

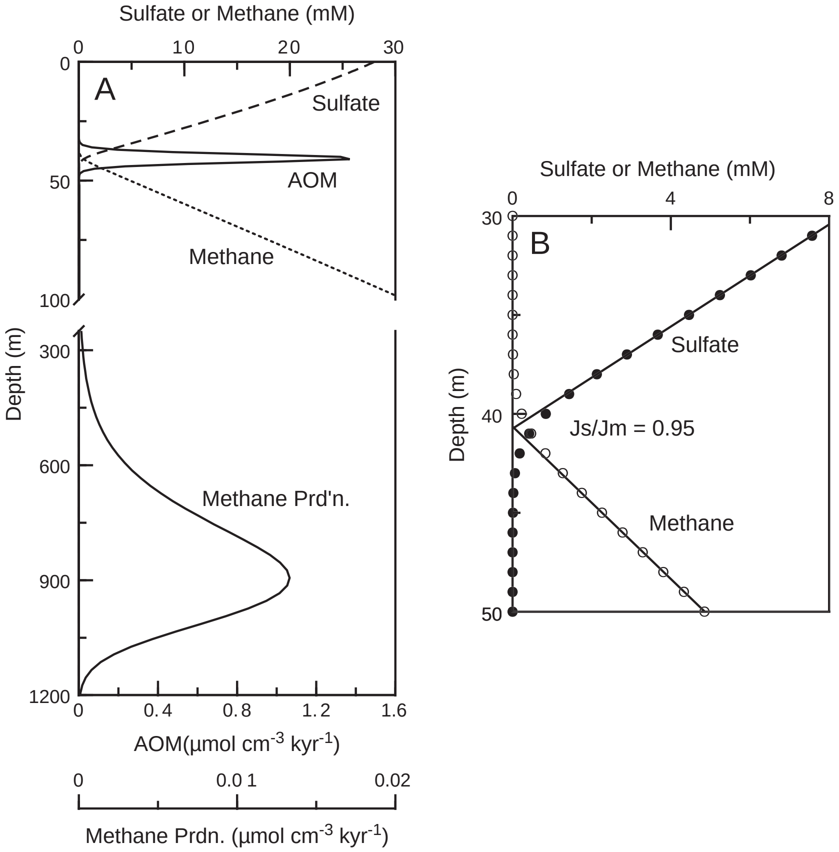

Fig. 7. (A) The effect of pore water advection on model-derived depth profiles of pore water sulfate and methane concentrations, and AOM and methane production rates. Here $u_o = -0.03$ m kyr^{-1} (i.e., advection is upwards), and all other model input parameters are listed in Table 1. (B) An expanded view around the SMTZ of the model-derived sulfate and methane concentration profiles shown in the left panel. The best-fit straight lines through the model data points (● and ○) just above and below the SMTZ were used to calculate the diffusive fluxes of sulfate and methane into the SMTZ.

the gross rate of pore water advection at the sediment surface (see Eq. (15)). Results with $u_o = -0.10$ m kyr^{-1} provide a good fit to the pore water sulfate data and reproduce the general trend in the methane data, although there is a ~5 m offset between the model-derived methane profile and the actual data. In contrast, results with $u_o = -0.06$ m kyr^{-1} more closely reproduce the methane data below the SMTZ, but predict a sulfate profile below ~10 m that is steeper than the actual data. At the present time it is difficult to ascertain the cause(s) of these differences.

These estimates of pore water advection are at low end of other model-derived estimates for Blake Ridge sediments that range from 0.12 to 0.25 m kyr^{-1} (Davie and Buffett, 2003a; Egeberg and Dickens, 1999; Wallmann et al., 2006). However, there are significant differences among these models both in terms of their formulation and structure, as well as the specific pore water solutes being examined in each case, making a direct comparison of these results difficult. Calculations using the model presented here with $u_o = -0.20$ m kyr^{-1} (results not shown), produce a sulfate profile that is far too steep than is observed in the pore water data, and a methane profile that is ~10 m offset above the actual data. These model results also predict that the upper boundary of the gas hydrate containing sediments occurs at 140 m sediment depth (versus the observed value of 190 m).

At the same time, two other aspects of the model results presented here agree well with observations from Blake Ridge sediments. The first is shown in the left panel of Fig. 8 where it can be seen that methane production peaks at a sediment depth of ~450 m. This agrees well with results which show that potential rates of microbial activity in Blake Ridge sediments increase dramatically below ~300 m, and that processes such as methanogenesis from bicarbonate (CO_2 reduction) show a broad maximum between 370 and 500 m (Wellsbury et al., 1997). It has been proposed that these maxima may be the result of microbial activity being stimulated around the base of the Blake Ridge hydrate-containing sediments at ~450 m (Wellsbury et al., 1997). However the results presented here suggest that increasing temperature with sediment depth and its effect on organic matter reactivity and remineralization is also a plausible explanation for this distribution of microbial activity in the deep region of these sediments.

The results in the right panel of Fig. 8 also show that the methane pore water profile intersects the methane solubility curve at a sediment depth of ~185 m (model run with $u_o = -0.10$ m kyr^{-1}) or ~210 m (model run with $u_o = -0.06$ m kyr^{-1}). Since methane gas hydrate is stable in Blake Ridge sediments at sediment depths above ~450 m, this cross-over point is the model-derived, upper boundary of hydrate-containing sediment. Results from ODP Leg 164 (Paull et al., 2000) suggest that this boundary occurs at a sediment depth of ~190 m, in excellent agreement with the model results presented here.

As noted above, an important question in the study of gas hydrates in sediments such as those on the Blake Ridge is the source of the methane found in the hydrates. Stable isotope results suggest a largely biogenic (rather than thermogenic) origin for this methane (Bohrmann and Torres, 2006). However, questions still remain as to whether this methane is: (1) produced in situ in or near the GHSZ; and/or (2) results from upward migration of biogenic methane (either as rising gas bubbles or as dissolved methane in the pore waters) from deeper ancient gas deposits, that then condenses to form gas hydrate when the methane reaches the GHSZ (Torres et al., 2004). Models in which organic matter degradation is assumed

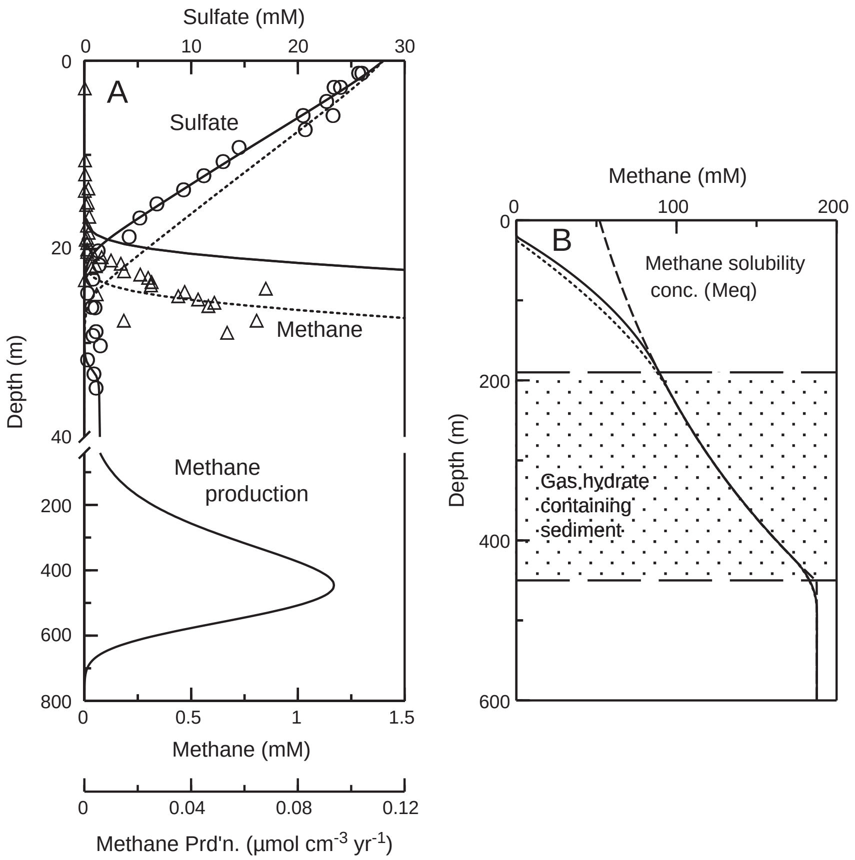

Fig. 8. (A) A fit of the model to sulfate (○) and methane (△) pore water data from ODP Leg 164, site 994 on the Blake Ridge (Borowski, 2004) for two values of u_o, -0.10 m kyr^{-1} (solid lines, model run BR-10) and 0.06 m kyr^{-1} (dotted lines, model run BR-12). All other model input parameters are listed in Table 3. Also shown here is the depth profile of methane production rate predicted by either model fit. (B) The complete model-derived pore water methane profiles based on the two fits to the Blake Ridge results shown in the left panel, and the depth distribution of the methane solubility concentration (M_{eq}) at this site (dashed line; calculated using the procedure described in Davie et al. (2004)). Note that the two model curves fit to the data intersect the methane solubility curve near ~190 m sediment depth which, as discussed in the text, defines the upper boundary of the gas hydrate containing sediments. The base of the gas hydrate stability zone is also shown at ~450 m.

to show a simple decrease in reactivity with increasing age or burial (Wallmann et al., 2006) largely favor the second explanation, in part because these models are unable to bury sufficient amounts of young, “labile” organic carbon deep enough in the sediments to minimize diffusive loss of methane versus incorporation into gas hydrate deposits. A variety of other approaches argue for at least some of the hydrate being formed in situ by methanogenesis in the GHSZ (Davie and Buffett, 2003b; Paull et al., 1994).

Table 3
Parameters used in the fit to the Blake Ridge results.[1]

Parameter	Value	Comments
G^0	10 mg C g_{dw}^{-1}	TOC values in Blake Ridge sediments range from ~10–23 mg C g_{dw}^{-1} (Paull et al., 1996).
ω_∞	0.051 m kyr^{-1}	This value was determined by assuming steady state compaction from the sediment surface to the base of the sediment column, i.e., $\omega_\infty = \omega_o(1-\varphi_o)/(1-\varphi_\infty)$ (see Section 3.1). The initial and final porosities (0.82 and 0.49 respectively) are defined below and ω_0 was taken to be 0.143 m kyr^{-1}, the average Holocene sedimentation rate for the Blake Ridge region (Borowski, 2004). Pliocene and Miocene sedimentation rates in the Blake Ridge region (sediment depths of several hundred meters) range from ~0.02 to 0.3 m kyr^{-1} (Borowski, 2004), consistent with this value of ω_∞.
u_o	-0.10 m kyr^{-1}	The “best fit” value for the sulfate data
	-0.06 m kyr^{-1}	The “best fit” value for the methane data (see Section 4.4 for details)
G_T	0.041 °C m^{-1}	The value used here was increased from the measured geothermal gradient (~0.036 °C m^{-1}) to adjust for the discrepancy between the depth of the bottom of the gas hydrate stability zone predicted by this lower geothermal gradient (~530 m) and the observed depth of this lower boundary at ~450 m (for details, see Davie and Buffett, 2003b).
k_T (2 °C)	1.11×10^{-5} kyr^{-1}	The average “best-fit” to the data for both u_o values. For specific fits with either u_o value this rate constant varied (relative to the value shown here) by$\pm$ 0.3×10^{-5} yr^{-1}.
k_{AOM}	10 mM^{-1} kyr^{-1}	From Hensen and Wallmann (2005).
k_{mr}	1 kyr^{-1}	This rate constant was set so that it is large enough to enforce thermodynamic equilibrium in the sediments (i.e., hydrate forms when the methane concentration is greater than or equal to M_{eq}) but not too large as to lead to instability in the numerical solution to the model equations (see related discussions in Davie and Buffett, 2001).
Ea	140 kJ mol^{-1}	The average “best-fit” to the data for both u_o values. For specific fits with either u_o value Ea varied (relative to the value shown here) by $\pm$50 kJ mol^{-1}.
BWT	3 °C	From Paull et al. (1996).
φ	0.49–0.82	Porosity data from site 994 (Paull et al., 1996) were fit to a double exponential function, yielding the following best-fit curve, $\varphi = 0.49 + 0.13e^{-0.421z} + 0.2e^{-0.0024z}$ ($r^2 = 0.721$, $n = 193$). Note that a double exponential provided a better fit to the field data than did the single exponential used in the other model results.

[1] All parameters are defined in Section 3.1.

In its current format, the model presented here is unable to critically examine all of these problems, in part because the model does not directly account for solid phase gas hydrate accumulation, nor does it consider gaseous methane fluxes from below the GHSZ. Nevertheless, calculations presented in Appendix A do allow me to examine at least some key aspects of this problem. These calculations suggest that in situ methanogenesis in Blake Ridge sediments can produce a steady-state inventory of ~20–40 Gt methane as gas hydrate. Estimates in the literature of this inventory range from 8 to 52 Gt methane (Torres et al., 2004), suggesting that in situ methanogenesis in the GHSZ can play an important role in supplying the methane found in Blake Ridge gas hydrates.

Based on arguments presented elsewhere (Davie and Buffett, 2001) steady-state models such as the one presented here are likely to reflect average environmental conditions in the sediments being examined on time scales of ~10^6 yr. However in many settings gas hydrates appear to be in non-steady state over 10s to 100s of thousands of years (Dickens, 2001; Hensen et al., 2003), often-times due to the response of the hydrate deposits to past climate change (Ruppel, 1997). Future studies using an expanded version of this model have the potential to address problems such as these, although the results presented here provide a reasonable and relatively straight-forward basic explanation for linkages between the deep marine biosphere, methane gas hydrates in marine sediments, and the occurrence of linear pore water sulfate profiles.

5. Conclusions

Assuming that the temperature dependence of sediment organic matter remineralization can be described by the Arrhenius equation, model results show that organic matter which is highly refractory at deep-sea seafloor temperatures (~2–3 °C) becomes reactive towards remineralization at sediment depths of several hundred meters due to burial and heating by the natural geothermal gradient. This results in a spatial separation between organic matter remineralization in near-surface sediments and remineralization in a deep reaction zone. In this deep reaction zone organic matter is degraded by methanogenesis, and above this there is a relatively large region in the sediments in which methane diffuses upwards to be oxidized by downward diffusing sulfate. Model calculations and field observations from outer continental margin sediments indicate that this sulfate methane transition zone (SMTZ) occurs at sediment depths of ~20 to >50 m, and sulfate profiles between the sediment surface and the SMTZ are often highly linear. These model calculations therefore provide a simple mechanistic explanation for the occurrence of linear pore water sulfate profiles that are common in many of these sediments. Linear sulfate gradients are often taken as an indirect indicator of gas hydrate occurrence although model results presented here suggest that this does not necessarily always have to be the case. This spatial separation of remineralization processes is in sharp contrast to nearshore marine sediments, where methanogenesis occurs immediately below the zone of sulfate reduction.

Application of the model developed here to gas hydrate-containing sediments on the Blake Ridge predicts pore water (methane and sulfate) profiles that are in good agreement with actual data. Model results predict a broad maximum in the rates of methanogenesis in these sediments at a sediment depth of ~400 m, consistent with measured potential rates of microbial processes in Blake Ridge sediments. An estimate of the upper boundary of the gas hydrate containing sediments based on these model results is in excellent agreement with field observations. Model results also suggest that in situ methanogenesis in the gas hydrate stability zone may play an important role in supplying the methane found in Blake Ridge gas hydrates. Continued development of this model should allow for a better understanding of the dynamics and biogeochemistry of gas hydrates.

In a more general sense, processes occurring in deeply-buried marine sediments appear to impact the global carbon and sulfur cycle on a number of different time scales (D'Hondt et al., 2002; Schrenk et al., 2010) although many of the details of how this occurs remain to be worked out. The model results presented here provide a mechanism by which surface organic matter fluxes can provide the energy required by microbial communities in deeply buried marine sediments. These observations should therefore greatly aid in furthering our understanding of these unique environments.

Acknowledgments

I would like to thank Amy Pitts for her assistance with some of the early model development. I also thank Walter Borowski and two anonymous reviewers for their extremely useful comments on an earlier version of this manuscript. Partial support for the preparation of this manuscript was provided by NSF (Chemical Oceanography Program).

Appendix A

To estimate the contribution of in situ methanogenesis to the methane found in gas hydrates in Blake Ridge sediments, I first estimate the residence time of material in the hydrate-containing region of the sediments (i.e., between sediments depths 190 m and 450 m). Assuming steady state compaction, the mass flux through the sediments will be constant with depth (see Eq. (13) and associated discussions), and therefore sediment input or removal to this region of the sediments is:

$$\omega_\infty(1-\varphi_\infty)\rho_{ds}A \tag{A.1}$$

where A is the sediment surface area on the Blake Ridge ($=26{,}000\ \mathrm{km}^2$; Dickens et al., 1997). The inventory of sediment in the gas hydrate-containing region of the sediments is approximately:

$$LA\left(1-\varphi_{avg}\right)\rho_{ds} \tag{A.2}$$

where $L=450–190=260$ m and $\varphi_{\rm avg}$ is the average porosity between sediment depths 190 and 450 m ($=0.58$). Dividing Eq. (A.2) by (A.1) yields τ, the residence time of material in the gas hydrate-containing region of the sediments, or

$$\tau=\frac{L}{\omega_\infty}\left(\frac{1-\varphi_{avg}}{1-\varphi_\infty}\right) \tag{A.3}$$

using the values listed here and in Table 3, $\tau=4240$ kyr.

Next, I estimate the depth-integrated in situ rate of methane gas hydrate production. In the model described in the text, methane in deep sediments is produced by methanogenesis and consumed by AOM; there is also an upward flux of methane into the model sediments from below the lower model boundary ($=800$ m) due to net upward pore water advection. The depth-integrated rate of methane production is given by:

$$DIMP=\varphi\int f_S k_T L_2 G\,dz \tag{A.4}$$

while the depth-integrated rate of AOM is,

$$DIAOM=\varphi\int k_{aom} SM\,dz \tag{A.5}$$

(see Eqs. (3)–(5) for details). Both integrals were solved by trapezoidal approximations using numerical model results and model input parameters in Table 3. The upward advective flux of dissolved methane is given by:

$$UMF = (\varphi_\infty \omega_\infty + u_o \varphi_o) M_{\max} \tag{A.6}$$

and again was determined with numerical model results and model input parameters in Table 3.

For model run BR-10 ($u_o = -0.1$ m kyr^{-1}), the values of DIMP, DIAOM, UMF are 28.9, 10.4 and 10.7 mmol m^{-2} yr^{-1} (respectively). For model run BR-12 ($u_o = -0.06$ m kyr^{-1}), these same values are 28.9, 8.7 and 4.6 mmol m^{-2} yr^{-1}.

The difference between DIMP + UMF and DIAOM is assumed here to represent methane that is "lost" due to hydrate formation (= GHF). In this calculation I initially assumed that methane produced in situ below the GHSZ (see Fig. 8) is eventually transported upwards into the GHSZ and incorporated into gas hydrate. With this assumption, GHF equals 29.2 mmol m^{-2} yr^{-1} (model run BR-10), with 73% of this hydrate formation resulting from in situ methanogenesis (versus upward advective flux from sediments below 800 m). For model run BR-12, GHF equals 24.8 mmol m^{-2} yr^{-1}, with 86% of this hydrate formation resulting from in situ methanogenesis. If, on the other hand, I assume that only methane produced within the hydrate-containing sediments (i.e., between the sediment depths 190 and 450 m) contributes to the gas hydrate inventory, then for both model runs the values of GHF are reduced by ~50%.

Finally, with these results the methane gas hydrate inventory in Blake Ridge sediments due to both in situ methanogenesis and upward advective flux of dissolved methane is given by,

$$GHF \times A \times \tau. \tag{A − 7}$$

For model run BR-10 ($u_o = -0.1$ m kyr^{-1}) this value is 51.5 Gt methane, while for run BR-12 ($u_o = -0.06$ m kyr^{-1}) it is 43.7 Gt methane. Interestingly however, when I separate out the relative contributions of in situ methanogenesis and upward advection from below 800 m, in situ methanogenesis in both cases is responsible for the production of ~40 Gt methane (37.6 and 37.7 Gt methane respectively). These values would be decreased roughly in half (~20 Gt CH_4) if I assume that only methane produced within the hydrate-containing sediments contributes to the gas hydrate inventory.

References

Aller, R.C., 1980. Diagenetic processes near the sediment–water interface of Long Island Sound, I. Decomposition and nutrient element geochemistry (S,N,P). Adv. Geophys. 22, 235–348.

Alperin, M.J., Hoehler, T.M., 2009. Anaerobic methane oxidation by archaea/sulfate-reducing bacteria aggregates: 1. Thermodynamic and physical constraints. Am. J. Sci. 309, 869–957.

Alperin, M.J., Reeburgh, W.S., Devol, A.H., 1992. Organic carbon remineralization and preservation in sediments of Skan Bay, Alaska. In: Whelan, J.K., Farrington, J.W. (Eds.), Productivity, Accumulation, and Preservation of Organic Matter in Recent and Ancient Sediments. Columbia Univ. Press, pp. 99–122.

Berelson, W.M., Prokopenko, M., Sansone, F.J., Graham, A.W., McManus, J., Bernhard, J.M., 2005. Anaerobic diagenesis of silica and carbon in continental margin sediments: discrete zones of TCO2 production. Geochim. Cosmochim. Acta 69, 4611–4629.

Berner, R.A., 1980. Early Diagenesis, a Theoretical Approach. Princeton University Press, Princeton, N.J.

Bohrmann, G., Torres, M., 2006. Gas hydrates in marine sediments. In: Schultz, H.D., Zabel, M. (Eds.), Marine Geochemistry. Springer, pp. 481–512.

Borowski, W.S., 2004. A review of methane and gas hydrates in the dynamic, stratified system of the Blake Ridge region, offshore southeastern North America. Chem. Geol. 205, 311–346.

Borowski, W., Paull, C., Ussler III, W., 1996. Marine pore-water sulfate profiles indicate in situ methane flux from underlying gas hydrate. Geology 24, 655.

Borowski, W.S., Paull, C.K., Ussler III, W., 1997. Carbon cycling within the upper methanogenic zone of continental rise sediments: an example from the methane-rich sediments overlying the Blake Ridge gas hydrate deposits. Mar. Geol. 57, 299–311.

Borowski, W.S., Paull, C.K., Ussler III, W., 1999. Global and local variations of interstitial sulfate gradients in deep-water, continental margin sediments: sensitivity to underlying methane and gas hydrates. Mar. Geol. 159, 131–154.

Borowski, W.S., Hoehler, T.M., Alperin, M.J., Rodriquez, N.M., Paull, C.K., 2000. Significance of anaerobic methane oxidation in methane-rich sediments overlying the Blake Ridge gas hydrate. In: Paull, C.K., Matsumoto, R., Wallace, P.J., Dillon, W.P. (Eds.), Proceedings ODP, Sci. Results, 164. TAMU, pp. 87–99.

Boudreau, B.P., 1997. Diagenetic Models and Their Implementation. Springer-Verlag, Berlin.

Boudreau, B.P., 2000. The mathematics of early diagenesis: from worms to waves. Rev. Geophys. 38, 389–416.

Boudreau, B.P., Ruddick, B.R., 1991. On a reactive continuum representation of organic matter diagenesis. Am. J. Sci. 291, 507–538.

Boudreau, B.P., Westrich, J.T., 1984. The dependence of bacterial sulfate reduction on sulfate concentrations in marine sediments. Geochim. Cosmochim. Acta 48, 2503–2516.

Buffett, B., Archer, D., 2004. Global inventory of methane clathrate: sensitivity to changes in the deep ocean. Earth Planet. Sci. Lett. 227, 185–199.

Burdige, D.J., 1991. The kinetics of organic matter mineralization in anoxic marine sediments. J. Mar. Res. 49, 727–761.

Burdige, D.J., 2006. Geochemistry of Marine Sediments. Princeton Univ. Press, Princeton.

Burdige, D.J., 2007. The preservation of organic matter in marine sediments: controls, mechanisms and an imbalance in sediment organic carbon budgets? Chem. Rev. 107, 467–485.

Burdige, D.J., Komada, T., 2011. Anaerobic oxidation of methane and the stoichiometry of remineralization processes in continental margin sediments. Limnol. Oceanogr. 56, 1781–1796.

Claypool, G.E., Kaplan, I.R., 1974. The origin and distribution of methane in marine sediments. In: Kaplan, I.R. (Ed.), Natural Gases in Marine Sediments. Plenum Press, pp. 99–139.

Cowie, G.L., Hedges, J.I., 1994. Biochemical indicators of diagenetic alteration in natural organic matter mixtures. Nature 369, 304–307.

Dale, A., Regnier, P., Knab, N., Jorgensen, B., Van Cappellen, P., 2008. Anaerobic oxidation of methane (AOM) in marine sediments from the Skagerrak (Denmark): II. Reaction-transport modeling. Geochim. Cosmochim. Acta 72, 2880–2894.

Davie, M.K., Buffett, B.A., 2001. A numerical model for the formation of gas hydrate below the seafloor. J. Geophys. Res. 106, 497–514.

Davie, M.K., Buffett, B.A., 2003a. A steady state model for marine hydrate formation: constraints on methane supply from pore water sulfate profiles. J. Geophys. Res. 108, 2495 2410.1029/2002JB002300.

Davie, M.K., Buffett, B.A., 2003b. Sources of methane for marine gas hydrate: inferences from a comparison of observations and numerical models. Earth Planet. Sci. Lett. 206, 51–63.

Davie, M.K., Zatsepina, O.Y., Buffett, B.A., 2004. Methane solubility in marine hydrate environments. Mar. Geol. 203, 177–184.

D'Hondt, S., Rutherford, S., Spivack, A.J., 2002. Metabolic activity of subsurface life in deep-sea sediments. Science 295, 2067–2070.

D'Hondt, S., Jørgensen, B.B., Miller, D.J., et al., 2005. Distributions of microbial activities in deep subseafloor sediments. Science 306, 2216–2221.

Dickens, G.R., 2001. Sulfate profiles and barium fronts in sediment on the Blake Ridge: present and past methane fluxes through a large gas hydrate resevoir. Geochim. Cosmochim. Acta 65, 529–543.

Dickens, G., Paull, C., Wallace, P., 1997. Direct measurement of in situ methane quantities in a large gas-hydrate reservoir. Nature 385, 426–428.

Egeberg, P.K., Dickens, G.R., 1999. Thermodynamic and pore water halogen constraints on gas hydrate accumulation at ODP site 997 (Blake Ridge). Chem. Geol. 153, 53–79.

Fehn, U., Snyder, G., Egeberg, P.K., 2000. Dating of pore waters with ^{129}I: relevance for the origin of marine gas hydrates. Science 289, 2332.

Froelich, P.N., Klinkhammer, G.P., Bender, M.L., Luedtke, N.A., Heath, G.R., Cullen, D., Dauphin, P., Hammond, D., Hartman, B., Maynard, V., 1979. Early oxidation of organic matter in pelagic sediments of the eastern equatorial Atlantic: suboxic diagenesis. Geochim. Cosmochim. Acta 43, 1075–1090.

Hedges, J.I., Keil, R.G., 1995. Sedimentary organic matter preservation: an assessment and speculative synthesis. Mar. Chem. 49, 81–115.

Hedges, J.I., Eglinton, G., Hatcher, P.G., Kirchman, D.L., Arnosti, C., Derenne, S., Evershed, R.P., Kogel-Knabner, I., de Leeuw, J.W., Littke, R., Michaelis, W., Rülkotter, J., 2000. The molecularly-uncharacterized component of nonliving organic matter in natural environments. Org. Geochem. 31, 945–958.

Hensen, C., Wallmann, K., 2005. Methane formation at Costa Rica continental margin—constraints for gas hydrate inventories and cross-décollement fluid flow. Earth Planet. Sci. Lett. 236, 41–60.

Hensen, C., Zabel, M., Pfeifer, K., Schwenk, T., Kasten, S., Riedinger, N., Schulz, H.D., Boetius, A., 2003. Control of sulfate pore-water profiles by sedimentary events and the significance of anaerobic oxidation of methane for the burial of sulfur in marine sediments. Geochim. Cosmochim. Acta 67, 2631–2647.

Hoehler, T.M., Borowski, W.S., Alperin, M.J., Rodriquez, N.M., Paull, C.K., 2000. Model, stable isotope, and radiotracer characterization of anaerobic methane oxidation in gas hydrate-bearing sediments of the Blake Ridge. Proc. ODP, Sci. Res. 164, 79–85.

X. Hu, Seagrass-Mediated Carbonate Dissolution and Early Diagenesis in Bahamas Bank Sediments, Ph.D. dissertation, Ph.D. dissertation, Old Dominion University, 2007.

Hunt, J.M., 1996. Petroleum Geochemistry and Geology. W.H. Freeman and Co., New York.

Jin, Q., Bethke, C.M., 2005. Predicting the rate of microbial respiration in geochemical environments. Geochim. Cosmochim. Acta 69, 1133–1143.

Jørgensen, B.B., Parkes, R.J., 2010. Role of sulfate reduction and methane production by organic carbon degradation in eutrophic fjord sediments (Limfjorden, Denmark). Limnol. Oceanogr. 55, 1338–1352.

Klump, J.V., Martens, C.S., 1989. The seasonality of nutrient regeneration in an organic rich coastal sediment: kinetic modelling of changing pore water-nutrient and sulfate distributions. Limnol. Oceanogr. 34, 559–577.

Lerman, A., 1977. Migrational processes and chemical reactions in interstitial waters. In: Goldberg, E.D. (Ed.), The Sea, 6. Wiley, New York, pp. 695–738.

Luff, R., Wallmann, K., 2003. Fluid flow, methane fluxes, carbonate precipitation and biogeochemical turnover in gas hydrate-bearing sediments at Hydrate Ridge, Cascadia Margin: numerical modeling and mass balances. Geochim. Cosmochim. Acta 67, 3403–3421.

Martens, C.S., Berner, R.A., 1974. Methane production in the interstitial waters of sulfate-depleted marine sediments. Science 185, 1167.

Martens, C.S., Albert, D.B., Alperin, M.J., 1998. Biogeochemical processes controlling methane in gassy coastal sediments — part 1. A model coupling organic matter flux to gas production, oxidation and transport. Cont. Shelf Res. 18, 1741–1770.

Meysman, F.J.R., Boudreau, B.P., Middelburg, J.J., 2005. Modelling reactive transport in sediments subject to bioturbation and compaction. Geochim. Cosmochim. Acta 69, 3601–3617.

Middelburg, J.J., 1989. A simple rate model for organic matter decomposition in marine sediments. Geochim. Cosmochim. Acta 53, 1577–1581.

Middelburg, J.J., Klaver, G., Nieuwenhuize, J., Wilemake, A., de Hass, W., Vlug, T., van der Nat, J.F.W.A., 1996. Organic matter mineralization in intertidal sediments along an estuarine gradient. Mar. Ecol. Prog. Ser. 132, 157–168.

Milkov, A.V., 2004. Global estimates of hydrate-bound gas in marine sediments: how much is really out there? Earth Sci. Rev. 66, 183–197.

Niewöhner, C., Hensen, C., Kasten, S., Zabel, M., Schulz, H.D., 1998. Deep sulfate reduction completely mediated by anaerobic methane oxidation in sediments of the upwelling area off Namibia. Geochim. Cosmochim. Acta 62, 455–464.

Parkes, R.J., Sass, H., 2009. Deep sub-surface. Encyclopedia of Microbiology. Academic Press, Oxford, pp. 64–79.

Parkes, R.J., Cragg, B.A., Bale, S.J., 1994. Deep bacterial biosphere in Pacific Ocean sediments. Nature 371, 410–413.

Parkes, R.J., Webster, G., Cragg, B.A., et al., 2005. Deep sub-seafloor prokaryotes stimulated at interfaces over geological time. Nature 436, 390–394.

Paull, C.K., Ussler, W., Borowski, W.S., 1994. Sources of biogenic methane to form marine gas hydrates: in situ production or upward migration? Ann. N. Y. Acad. Sci. 715, 392–409.

Paull, C.K., Matsumoto, R., Wallace, P., et al., 1996. Proc. ODP, Init. Repts, 164. Ocean Drilling Program, College Station, TX.

Paull, C.K., Matsumoto, R., Wallace, P.J., Dillon, W.P. (Eds.), 2000. Proc. ODP, Sci. Results, 164. Ocean Drilling Program, TX.

Reeburgh, W.S., 2007. Oceanic methane biogeochemistry. Chem. Rev. 107, 486–513.

Rempel, A.W., Buffett, B.A., 1997. Formation and accumulation of gas hydrate in porous media. J. Geophys. Res. 102 (B5), 10151–10164.

Robador, A., Brüchert, V., Jørgensen, B.B., 2009. The impact of temperature change on the activity and community composition of sulfate reducing bacteria in arctic versus temperate marine sediments. Environ. Microbiol. 11, 1692–1703.

Roussel, E., Bonavita, M., Querellou, J., Cragg, B., Webster, G., Prieur, D., Parkes, R., 2008. Extending the sub-sea-floor biosphere. Science 320, 1046.

Roychoudhury, A.N., Viollier, E., Van Capellen, P., 1998. A plug flow-through reactor for studying biogeochemical reactions in undisturbed sediments. Appl. Geochem. 13, 269–280.

Rullkötter, J., 2006. Organic matter: the driving force for early diagenesis. In: Schulz, H.D., Zabel, M. (Eds.), Marine Geochemistry. Springer-Verlag, Berlin.

Ruppel, C., 1997. Anomalously cold temperatures observed at the base of the gas hydrate stability zone on the US Atlantic passive margin. Geology 25, 699.

Schiesser, W.E., 1991. The Numerical Method of Lines: Integration of Partial Differential Equations. Academic Press, San Diego. 326 pp.

Schrenk, M.O., Huber, J.A., Edwards, K.J., 2010. Microbial provinces in the subseafloor. Ann. Rev. Mar. Sci. 2, 279–304.

Schulz, H.D., Zabel, M. (Eds.), 2006. Marine Geochemistry. Springer-Verlag, Berlin.

Sivan, O., Schrag, D.P., Murray, R.W., 2007. Rates of methanogenesis and methanotrophy in deep sea sediments. Geobiology 5, 141–151.

Torres, M., Wallmann, K., Trehu, A., Bohrmann, G., Borowski, W., Tomaru, H., 2004. Gas hydrate growth, methane transport, and chloride enrichment at the southern summit of Hydrate Ridge, Cascadia margin off Oregon. Earth Planet. Sci. Lett. 226, 225–241.

Wallmann, K., Aloisi, G., Haeckel, M., Obzhirov, A., Pavlova, G., Tishchenko, P., 2006. Kinetics of organic matter degradation, microbial methane generation, and gas hydrate formation in anoxic marine sediments. Geochim. Cosmochim. Acta 70, 3905–3927.

Wang, G., Spivack, A., Rutherford, S., Manor, U., D'Hondt, S., 2008. Quantification of co-occurring reaction rates in deep subseafloor sediments. Geochim. Cosmochim. Acta 72, 3479–3488.

Wellsbury, P., Goodman, K., Barth, T., Cragg, B.A., Barnes, S.P., Parkes, R.J., 1997. Deep marine biosphere fuelled by increasing organic matter availability during burial and heating. Nature 388, 573–576.

Weston, N.B., Joye, S.B., 2005. Temperature-driven decoupling of key phases of organic matter degradation in marine sediments. Proc. Nat. Acad. Sci. U. S. A. 102, 17036–17040.

Westrich, J.T., Berner, R.A., 1984. The role of sedimentary organic matter in bacterial sulfate reduction: the G model tested. Limnol. Oceanogr. 29, 236–249.

Westrich, J.T., Berner, R.A., 1988. The effect of temperature on rates of sulfate reduction in marine sediments. Geomicrobiol. J. 6, 99–117.

Whitman, W.B., Coleman, D.C., Wiebe, W.J., 1998. Prokaryotes: the unseen majority. Proc. Natl. Acad. Sci. 95, 6578–6583.

Wortmann, U., 2006. A 300 m long depth profile of metabolic activity of sulfate-reducing bacteria in the continental margin sediments of South Australia (ODP Site 1130) derived from inverse reaction-transport modeling. Geochem. Geophys. Geosyst. 7, Q05012.

Xu, W., Ruppel, C., 1999. Predicting the occurence, distribution and evolution of methane gas hydrate in porous marine sediments. J. Geophys. Res. 104 (B3), 5081–5095.